

1 **Exploring impacts of forest management strategies on water partitioning in a drought-sensitive catchment**  
2 **using a tracer-aided ecohydrological framework**

3 Cong Jiang <sup>1</sup>, Doerthe Tetzlaff <sup>1,2,3</sup>, Songjun Wu<sup>1</sup>, Christian Birkel <sup>1,4</sup>, Hjalmar Laudon <sup>5</sup>, Chris Soulsby <sup>1,3,5,6</sup>

4 <sup>1</sup> Leibniz-Institute of Freshwater Ecology and Inland Fisheries (IGB), Department of Ecohydrology and  
5 Biogeochemistry, Berlin, Germany

6 <sup>2</sup> Department of Geography, Humboldt University Berlin, Berlin, Germany

7 <sup>3</sup> Northern Rivers Institute, University of Aberdeen, Aberdeen, UK

8 <sup>4</sup> Department of Geography, University of Costa Rica, San Pedro, Costa Rica

9 <sup>5</sup> Department of Forest Ecology and Management, Swedish University of Agricultural Science (SLU), Sweden

10 <sup>6</sup> Chair of Water Resources Management and Modeling of Hydrosystems, Technical University Berlin, Berlin,  
11 Germany

12 *Correspondence to:* Cong Jiang (cong.jiang@igb-berlin.de)

13 **Abstract.** Land use strongly influences water partitioning, water availability, and ecohydrological resilience in  
14 drought-sensitive regions. Forest management plays a critical role through its effects on water use, which depend  
15 on forest type, forest density, root water uptake, yet the ecohydrological consequences of different forest  
16 management strategies—particularly in terms of blue and green water fluxes—remain poorly quantified. Here,  
17 we develop and apply a parsimonious, tracer-aided forest management scenario framework using the conceptual  
18 ecohydrological model EcoPlot-iso, designed to isolate the dominant vegetation-structural controls on long-term  
19 water partitioning. We investigated how variations in generic forest type (e.g., broadleaf vs. conifer), forest density,  
20 and root distribution influence water partitioning and ecohydrological resilience under different wetness  
21 conditions in the drought-sensitive lowland Demnitzer Millcreek catchment (DMC), northeastern Germany.  
22 Baseline simulations for the period 2000–2024 were conducted at three forest sites and used to develop forest-  
23 type-specific reference conditions for comparison with alternative forest management scenarios. A key innovation  
24 in this version of EcoPlot-iso was the integration of a depth-dependent root water uptake function, allowing  
25 simulation of transpiration across soil layers with contrasting rooting distribution and stand ages. The model was  
26 calibrated and validated using seven years of soil moisture and three years of soil water isotope ( $\delta^2\text{H}$ ) data through  
27 a multi-criteria approach. Results showed that, on average, evapotranspiration was highest under conifers,  
28 exceeding broadleaf forests and agroforestry by 7% and 11%, respectively, while agroforestry exhibited the  
29 greatest groundwater recharge. Significant differences in water partitioning between dry and wet years were  
30 observed across management scenarios. Comparisons between wet and dry years indicate that conifer forests show  
31 the strongest transpiration contrasts relative to broadleaf forests in early spring, while peak drought sensitivity  
32 occurs in late spring. Our findings highlight the potential of agroforestry, such as crop–tree mixtures, to mitigate  
33 drought impacts. Overall, this study demonstrates how a parsimonious, tracer-aided scenario framework can be  
34 used as a decision-support tool to quantify and visualize the effects of land use change on water availability in  
35 data-limited regions, supporting more informed decision-making and enhanced ecohydrological resilience under  
36 increasing drought pressure.

37

## 38 **1 Introduction**

39 Land use plays a crucial role in regulating water, carbon, energy, and nutrient cycles by mediating ecohydrological  
40 fluxes and soil water storage dynamics which link interactions between the atmosphere, soils, vegetation and  
41 biogeochemical processes (Mahmood et al., 2014; Pielke et al., 2011; Smith et al., 2021; Sterling et al., 2013).  
42 Among the different types of land cover, forests are particularly important elements of the land use mosaic,  
43 providing a range of ecosystem services, including enhancing infiltration, stabilizing soils, storing carbon,  
44 supplying timber and fuelwood, as well as buffering extreme climate events (Bonan, 2008). However, there are  
45 clear trade-offs, as forests and trees also tend to use more water than contrasting land uses (Bosch & Hewlett,  
46 1982; Calder, 1998). This is because their high Leaf Area Index (LAI) and canopy storage capacities often result  
47 in greater interception losses and canopy evaporation, while their deeper and denser rooting networks can sustain  
48 transpiration when top soils dry out (Wang-Erlandsson et al., 2014). Consequently, forest management decisions,  
49 (e.g., afforestation, thinning, forest type selection etc.) can significantly affect water yield, the partitioning into  
50 blue (runoff, groundwater recharge) and green (evapotranspiration) water fluxes, and the ecohydrological  
51 resilience to drought; defined here as the ability of soil–plant–water system to sustain key hydrological and  
52 ecological functions under drought stress (Falkenmark & Rockström, 2006; Neill et al., 2021; Tetzlaff et al., 2024).

53 Sustainable land management also requires consideration of sensitivity to climate change, which is altering  
54 hydroclimatic regimes by shifting precipitation patterns and increasing atmospheric moisture demand (Huntington,  
55 2006; Trenberth, 2011). These changes can intensify drought frequency and duration, increase evaporative losses,  
56 and reduce groundwater recharge and surface water availability, and thus exacerbating water scarcity in many  
57 regions (Ault, 2020; Yuan et al., 2023). Because land use practices—particularly forest management—are  
58 expected to strongly influence water partitioning, it is important to assess their impacts under changing  
59 hydroclimatic conditions in order to evaluate the ecohydrological resilience of soil–plant–water systems,  
60 especially in drought-sensitive areas.

61 The understanding of how land use change affects runoff generation, soil moisture storage and evapotranspiration  
62 dynamics has gradually developed through decades of research, including long-term paired experimental  
63 watershed investigations of water yield (Bosch & Hewlett, 1982; Brown et al., 2005, 2013; Hibbert, 1967).  
64 However, quantifying the impact of forest management on water partitioning remains challenging in most  
65 situations (Guswa et al., 2020). This is due to the complex interplay of climate conditions, soil properties,  
66 vegetation type, and topography, and the difficulty in distinguishing individual evapotranspiration (ET)  
67 components (Kool et al., 2014; Smith et al., 2021; Zhang et al., 2001). These challenges are further compounded  
68 by scarce long-term observational data for forest ecosystems, which are essential given their slow dynamics and  
69 lengthy growth cycles (Tetzlaff et al., 2017).

70 In forest ecosystems, ET is particularly challenging to simulate due to complex interactions among canopy  
71 structure, stomatal behavior, and root water uptake (Tague & Band, 2004). Many ecohydrological models include  
72 some form of root water uptake parameterization (e.g., mHM, EcH2O-iso), in which canopy transpiration is  
73 typically constrained by surface energy balance and stomatal conductance and subsequently distributed among  
74 soil layers based on soil water availability and root distribution. While such models provide detailed  
75 representations of land–atmosphere and soil–vegetation interactions, their application in forest management  
76 studies is often constrained by high data requirements, computational demand, and parameter uncertainty,

77 particularly in data-scarce regions (Fatichi et al., 2012; Ricci et al., 2020; Tague & Band, 2004). In this context,  
78 conceptual tracer-aided ecohydrological models can provide a complementary, process-based, and practical  
79 framework for systematically exploring long-term forest management impacts on water partitioning and  
80 ecohydrological resilience (Landgraf et al., 2023). By integrating climatic forcing, canopy structure (e.g., leaf area  
81 index), soil moisture dynamics, and stable water isotopes, such approaches facilitate robust assessment of green-  
82 and blue-water fluxes under contrasting forest management scenarios (Neill et al., 2021).

83 In this study, we apply the tracer-aided conceptual model EcoPlot-iso to assess how land use, specifically forest  
84 management strategies, influences water partitioning and soil moisture storage in the drought-sensitive, lowland  
85 Demnitzer Millcreek catchment, NE Germany. This lowland catchment is typical of large areas in central Europe  
86 where freely draining, sandy soils combine with a relatively low precipitation, and high evaporative demand  
87 amplify drought stress under climate change. To improve the quantification of transpiration, we introduce a novel  
88 development in EcoPlot-iso by integrating a depth-dependent root water withdrawal function into the transpiration  
89 equation. The model is dual-calibrated and validated using seven years of soil moisture data and three years of  
90 soil water isotope data. A series of generic forest management scenarios — varying broad forest types (broadleaf,  
91 coniferous, agroforestry), forest density, and rooting characteristics — are developed within a parsimonious,  
92 tracer-aided forest management scenario framework, to explore their impacts on vertical water fluxes and  
93 ecohydrological resilience.

94 This study aims to answer the following research questions:

- 95       ➤ How does vegetation cover influence water use and partitioning under varying wetness conditions  
96       in a drought-sensitive, lowland catchment?
- 97       ➤ What are the implications of alternative generic forest management scenarios for water availability  
98       and overall ecohydrological resilience?
- 99       ➤ How can we optimize the land management strategies to mitigate drought impacts and enhance  
100      ecohydrological resilience in the face of climate change?

## 101 **2 Study area**

### 102 **2.1 Demnitzer Millcreek catchment (DMC)**

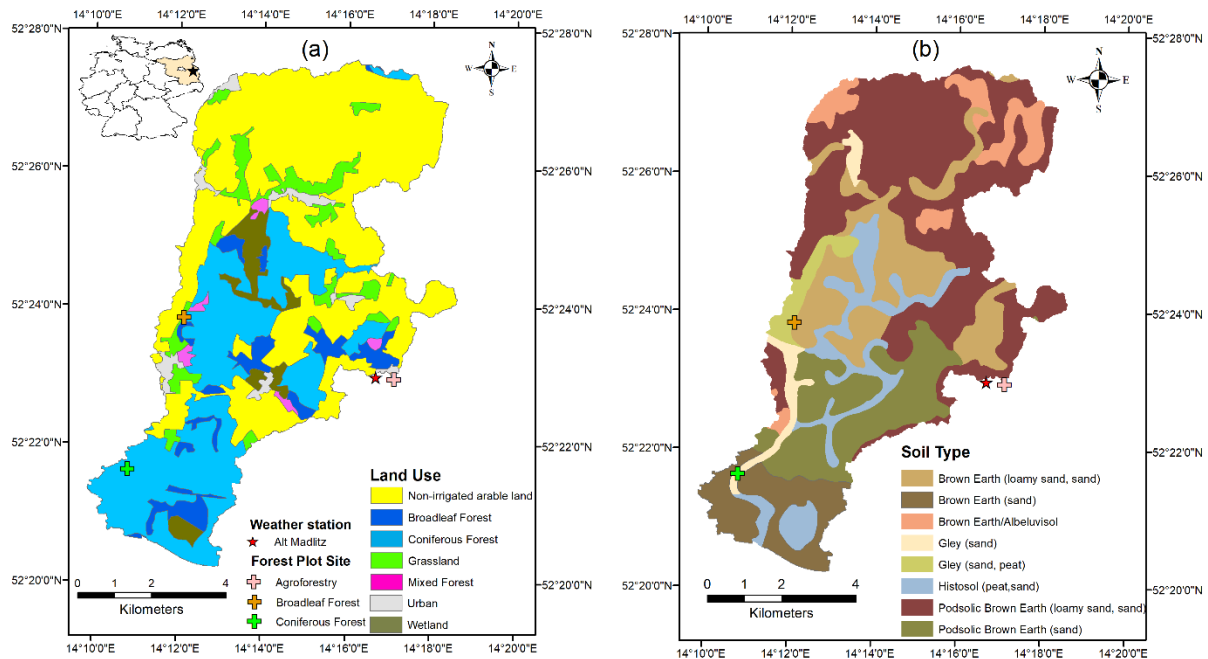
103 The Demnitzer Millcreek catchment (DMC) is a 66 km<sup>2</sup> lowland basin (30–90 m elevation) in the State of  
104 Brandenburg, Germany, approximately 55 km east of Berlin (52°23' N, 14°15' E) (Fig. 1). Located in the Northern  
105 European Plain, it is part of a drought-sensitive region that provides many essential ecosystem services, including  
106 agriculture, timber production, and water supply.

107 The DMC landscape is dominated by non-irrigated farmland, mostly arable crops and some grazing on more  
108 water-retentive soils brown and gley soils respectively which cover 60% of the catchment (Fig. 1a and b). Forests  
109 cover 36% of the catchment on more freely draining sandy soils, and include coniferous, broadleaf, and mixed  
110 stands. Small urban settlements (2%) are scattered throughout the catchment, with wetlands on peat soils primarily  
111 found along streams in the central part of the catchment. The climate is temperate with warm summers, with a  
112 mean annual temperature of 9.6°C and average precipitation of approximately 558 mm, based on weather station

113 data from 2000 to 2024. Potential evapotranspiration (PET) ranges from 584 to 789 mm per year from 2000 to  
114 2024, based on calculations from this study (see Section 3.3). Interannual variability in precipitation, including  
115 the identification of dry and wet years, is shown in Fig. S1, which highlights deviations from the long-term mean  
116 and helps contextualize recent drought impacts. Rainfall peaks in summer, accompanied by intense convective  
117 storms; however, surface runoff is rare, as the soils are highly permeable and dry in the growing season.  
118 Consequently, the catchment is primarily groundwater-dominated with winter high flows and often dries in the  
119 summer (Smith et al., 2021). The geology consists mainly of glacial and fluvial deposits and base moraines, while  
120 the dominant soil types include poorly drained silty gley brown earth and well-drained podzolic brown earth soils  
121 (Fig. 1b).

122 The DMC has a long history of human influence, with significant land use changes affecting its hydrology. In the  
123 18<sup>th</sup> Century, artificial drainage channels were constructed to convert wetlands into agricultural land. Since the  
124 1990s, efforts in wetland restoration and wildlife recolonization (e.g., beaver recovery) have aimed to enhance  
125 water retention in the landscape. Long-term hydrological and isotopic monitoring (Gelbrecht et al., 1996, 2005;  
126 Smith et al., 2020; Wu et al., 2021) has provided valuable insights into the impacts of agriculture and land use  
127 management on water quality, ecohydrological partitioning and soil water storage. The 2018 European drought  
128 and subsequent prolonged dry periods have exacerbated water scarcity and ecosystem vulnerability (Kleine et al.,  
129 2021). In response, some land owners have explored agroforestry and other adaptive forest and tree management  
130 strategies to improve water retention and landscape resilience (Luo et al., 2024). Agroforestry represents a  
131 transitional system blending low density tree cultivation and with agriculture; either in terms of grazing the  
132 understory vegetation or crops (Landgraf et al., 2022; Quandt et al., 2023). Given the long-term monitoring record  
133 and ongoing land use change, DMC serves as a useful site for assessing the impacts of changing forest  
134 management on water partitioning, soil moisture and ecohydrological resilience under different wetness  
135 conditions.

136



137  
 138 **Figure 1.** Location, land use (a) and soil type (b) map of the Demnitzer Millcreek catchment, showing the current  
 139 distribution of broadleaf forests, conifer forests, agroforestry, cropland, and grassland.

140 **2.2 Forest Plot Sites**

141 To investigate the effects of forest management scenarios on water partitioning and ecohydrological resilience,  
 142 three predominantly forest plot sites — broadleaf forest, conifer forest and agroforestry — were selected within  
 143 the drought-sensitive DMC. These plots represent contrasting forest type central to the modelling experiments.  
 144 The plot locations are shown in Fig. 1, and key site characteristics are summarized below, with further details  
 145 available in Kleine et al. (2021) and Landgraf et al. (2023). A summary of observed soil types and soil moisture  
 146 monitoring characteristics for these three forest sites is provided in Table 1, which also highlights pronounced  
 147 differences in long-term mean volumetric soil moisture averaged over the 0–1 m soil profile, with values highest  
 148 in agroforestry (~21%), intermediate in broadleaf (~11%), and lowest in conifer forest (~5.5%).

149 The broadleaf forest site represents a relatively mature forest system (~60 years old) and is dominated by mature  
 150 European oak (*Quercus robur*) with a few Scots pine (*Pinus sylvestris*) present within the plot. Additional species  
 151 including Norway maple (*Acer platanoides*), elm (*Ulmus* spp.), and hazel (*Corylus avellana*) are found within  
 152 10 m of the plot boundary. The soil is classified as Brown Earth, with a loamy sand to sand texture.

153 The conifer forest site is structurally simpler and more homogeneous, and is dominated by mature Scots pine  
 154 (*Pinus sylvestris*) plantation. A limited number of broadleaf species, such as European oak and Norway maple,  
 155 are also present within the plot, reflecting a conifer-dominated canopy. The soil is a weakly developed brown  
 156 earth, characterized by coarse sandy texture and overlying gravels.

157 The agroforestry site represents a transitional system between forest and agriculture and is characterized by  
 158 minimal canopy cover and no irrigation. It consists of rows of small deciduous trees or shrubs ( $\leq 2$  m in height),  
 159 spaced approximately 2–3 m apart, interplanted with rainfed legumes (Landgraf et al., 2023). The soil is classified  
 160 as podsolc brown earth, with a loamy sand to sand texture.

161 Together, these three sites represent a realistic gradient of forest land use intensity and provide a basis for  
 162 exploring how forest type, forest density, and rooting depth affect ecohydrological responses under varying  
 163 climatic conditions.

164 **Table 1.** Summary of observed soil types and soil moisture data at the three forest sites.

Site	Soil Type	Texture	Layer	Soil Moisture (mm)				Period
				Max	Min	Mean	SD	
Broadleaf forest	Brown earth	Loamy sand/sand	0 to 10 cm	26.3	3.5	13.7	6.3	2018.6-2024.12
			10 to 30 cm	56.2	6.9	24.7	11.7	
			30 to 100 cm	147.5	25.8	71.7	33.5	
Conifer forest	Sandy brown earth	Coarse sand	0 to 10 cm	28.7	8.6	17.3	7.1	2019.3-2024.12
			10 to 30 cm	53.8	2.6	21.8	12.3	
			30 to 100 cm	34.7	2.7	15.9	8.0	
Agroforestry	Podsollic brown earth	Loamy sand/sand	0 to 10 cm	32.1	10.4	21.3	7.8	
			10 to 30 cm	53.4	7.2	29.8	13.5	
			30 to 100 cm	223.6	86.8	163.4	42.0	

### 165 3 Method and Data

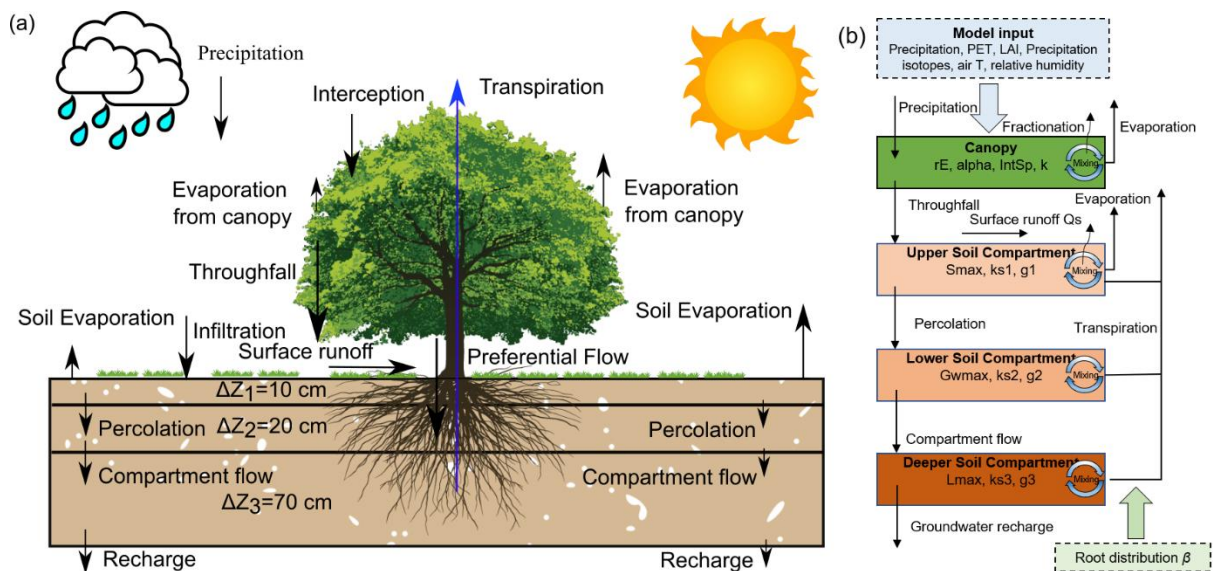
#### 166 3.1 Model Framework and Structure

167 This study employs the EcoPlot-iso model, a tracer-aided ecohydrological modelling framework designed to  
 168 simulate key ecohydrological and isotopic processes that characterise water partitioning at the plot scale (Birkel  
 169 et al., 2024; Landgraf et al., 2023; Stevenson et al., 2023). EcoPlot-iso is a process-based conceptual model that  
 170 simulates key ecohydrological fluxes, including interception, throughfall, infiltration, preferential flow, surface  
 171 runoff, percolation, and groundwater recharge, as well as evapotranspiration components such as canopy  
 172 evaporation, soil evaporation, and transpiration (Fig. 2a). These processes are represented within a vertical  
 173 structure comprising a single canopy layer and three soil layers (0–10 cm, 10–30 cm, and 30–100 cm) (Fig. 2b).  
 174 The vertical discretization follows the established EcoPlot-iso configuration and effectively represents vertical  
 175 gradients in soil moisture and isotopic composition, broadly consistent with soil moisture and isotope  
 176 measurements within each layer. Recently, the isotope tracking module was further developed to include  
 177 fractionation and mixing processes, allowing EcoPlot-iso to better constrain the partitioning between evaporation  
 178 and transpiration and improve water flux estimates. The required input variables (Table 2) include meteorological  
 179 data such as precipitation, potential evapotranspiration (PET), air temperature, and relative humidity, along with  
 180 stable water isotopic data (precipitation isotope) and vegetation-related parameters (leaf area index, LAI).

181 In EcoPlot-iso, canopy surface cover fraction (SCF) is derived from LAI using Beer’s law with an extinction  
 182 coefficient  $rE$  (Eq. S1). Maximum canopy storage is determined by the SCF and an interception threshold  
 183 parameter  $\alpha$ . Interception is represented by a nonlinear saturation-type function (Eq. S2), whereby precipitation is  
 184 first stored in the canopy until maximum canopy storage is reached, and any excess is routed as throughfall.  
 185 Potential evapotranspiration PET is partitioned into canopy and soil fractions according to SCF (Eqs. S3 and S4).  
 186 The canopy fraction drives evaporation from the interception store and transpiration from the soil layers, while  
 187 the soil fraction drives evaporation from the upper soil layer (Eqs. S5–S6). Actual fluxes are constrained by water  
 188 availability: interception evaporation depends on canopy storage, transpiration is sequentially satisfied from the  
 189 upper to deeper soil layers according to the relative soil-moisture availability (STO/Smax) of each layer (Eqs. S7–

190 S9), and soil evaporation is limited by moisture availability in the upper soil. Surface runoff is represented using  
 191 a Hortonian threshold approach, where precipitation in excess of infiltration capacity is routed as runoff (Eq. S10).  
 192 Preferential flow is triggered when throughfall exceeds a threshold, with a calibrated parameter controlling the  
 193 bypass proportion (Eq. S11). Percolation, compartment flow and groundwater recharge are represented as storage–  
 194 discharge relationships, where outflows are parameterised as power functions of soil or groundwater storage (Eqs.  
 195 S12-S14). Groundwater recharge is defined as the downward percolation flux at the lower boundary of the soil  
 196 domain (30–100 cm layer), corresponding to a total soil depth of 1 m. Full variable definitions and governing  
 197 equations are provided in Table S1 of the Supplementary Material (Eqs. S1–S14).

198 EcoPlot-iso has been applied in diverse climatic and hydrological settings, including a one-year simulation in  
 199 Scotland (Stevenson et al., 2023), a one-year simulation at the Demnitzer Millcreek (DMC) site in the Northern  
 200 European Plain (Landgraf et al., 2023), and a four-year simulation in the humid tropics of Costa Rica (Birkel et  
 201 al., 2024). Building on these applications, this study employs EcoPlot-iso for a long-term tracer-aided  
 202 ecohydrological simulation to assess the effects of different forest management scenarios on water partitioning  
 203 and ecohydrological resilience.



204  
 205 **Figure 2.** (a) Schematic representation of the ecohydrological fluxes and water partitioning in the EcoPlot-iso  
 206 model illustrating major water fluxes and storage components; (b) Conceptual framework and key parameters of  
 207 the EcoPlot-iso model (Landgraf et al., 2023; Stevenson et al., 2023), highlighting the key ecohydrological  
 208 processes simulated in this study.

### 209 3.2 Model Adaptations: Integrating Root Distribution into the Transpiration Equation

210 Although root water uptake plays a critical role in soil–plant–atmosphere interactions, the vertical rooting  
 211 distribution and the associated depth-dependent uptake efficiency was not explicitly represented in EcoPlot-iso  
 212 (Stevenson et al., 2023). The current study introduces a novel depth-dependent root uptake function to improve  
 213 the model’s simulation of transpiration and water partitioning across different root distributions. This adaptation  
 214 enables the model to account for variations in rooting depth and water uptake efficiency across land use types—  
 215 such as young and mature forests or contrasting vegetation covers—that affect soil water extraction. Specifically,  
 216 a new transpiration equation was implemented to calculate root water uptake across three soil compartments—  
 217 shallow, middle, and deep—by incorporating depth-specific uptake efficiency:

$$218 \quad T_{p1} = r_{L1} * (T_P - E_i) * \left( \frac{STO}{S_{max}} \right) \quad (1)$$

$$219 \quad T_{p2} = r_{L2} * (T_P - E_i - T_{p1}) * \left( \frac{GW}{GW_{max}} \right) \quad (2)$$

$$220 \quad T_{p3} = r_{L3} * (T_P - E_i - T_{p1} - T_{p2}) * \left( \frac{SDeep}{SDeep_{max}} \right) \quad (3)$$

221 where  $T_{p1}$ ,  $T_{p2}$ ,  $T_{p3}$  represent the transpiration from the upper, lower, and deeper soil compartments, respectively.  
 222  $E_i$  denotes the canopy evaporation.  $STO$ ,  $GW$ ,  $SDeep$  represent the water storage in the upper, lower, and deeper  
 223 soil compartments.  $S_{max}$ ,  $GW_{max}$ ,  $SDeep_{max}$  are the maximum water storage capacities of these compartments.  $r_{L1}$ ,  
 224  $r_{L2}$  and  $r_{L3}$  represent the root water withdrawal efficiency in the upper, lower, and deeper soil compartments,  
 225 respectively.

226 To explicitly link root water uptake to soil moisture availability and transpiration demand, an efficiency factor  $r(z)$   
 227 was introduced. The exponential root water withdrawal efficiency function is defined as:

$$228 \quad r(z) = e^{-\beta z} \quad (4)$$

229 where  $r(z)$  represents the capacity of roots to extract water at depth  $z$ , and  $\beta$  is the decay rate, which determines  
 230 how quickly root activity decreases with increasing depth. A higher  $\beta$  value concentrates root activity near the  
 231 surface, while lower  $\beta$  values allow for deeper water uptake (see Fig. S2 in Supplement). This formulation builds  
 232 on the common assumption that potential root water uptake decreases exponentially with depth (Li et al., 1999;  
 233 Wu et al., 1999) and is intentionally simplified for a plot-scale, data-constrained model setup. The soil profile is  
 234 discretized into three layers (0–10 cm, 10–30 cm, and 30–100 cm; Fig. 2a), and  $rL1$ ,  $rL2$ , and  $rL3$  are calculated  
 235 by evaluating  $r(z)$  at the midpoint depth of each layer ( $z = 5, 20$ , and  $65$  cm, respectively). These layer-specific  
 236 efficiency values are then used as weighting coefficients in Eqs. (1)–(3) to calculate transpiration from each of  
 237 the three soil compartments.

### 238 3.3 Model Setup and Input and Observation Data

239 The EcoPlot-iso model was applied to DMC across five sites with different dominant land use: broadleaf forest,  
 240 conifer forest, agroforestry, cropland and grassland over a 25-year period (2000–2024) at daily timesteps. Soil  
 241 moisture initialization was based on observed data, and a one-year spin-up period was included before each  
 242 simulation to stabilize initial conditions. The input datasets required for the model—climate, vegetation, soil  
 243 moisture, and stable water isotope data—are summarized in Table 2. Climate variables, including precipitation,  
 244 temperature, wind speed, and relative humidity, were primarily obtained from the Müncheberg weather station  
 245 (DWD, German Weather Service, ~20 km from DMC). Potential Evapotranspiration (PET) was calculated using  
 246 the FAO Penman-Monteith equation, while net radiation was derived from ERA5 reanalysis data (Hersbach et al.,  
 247 2020). The Leaf Area Index (LAI) time series was extracted from the MODIS 8-day LAI product at the location  
 248 of each study site and linearly interpolated to daily timesteps. To improve accuracy and reduce data noise, the  
 249 MODIS LAI was further bias-corrected against in-situ LAI measurements (maximum and minimum values),

250 following Smith et al. (2021) and Wu et al. (2023). Given the plot-scale setup of EcoPlot-iso, agroforestry systems,  
 251 characterized by mixed crop–tree vegetation, are represented implicitly using MODIS-derived LAI and calibration  
 252 against plot-scale soil moisture and isotope observations, rather than explicitly resolving multiple vegetation types.  
 253 In addition, the complete set of time series input data used to drive the EcoPlot-iso simulations in the Demnitzer  
 254 MillCreek Catchment for 2000–2004—including daily precipitation, precipitation isotopes ( $\delta^2\text{H}$ ), air temperature,  
 255 relative humidity, Leaf Area Index (LAI), and potential evapotranspiration (PET)—is presented in Figure S3 of  
 256 the Supplementary Material.

257 Surface soil moisture (0–10 cm) was measured using a handheld soil moisture device (Theta handheld probe ML3  
 258 Sensor) on a monthly basis during two field observation periods (2018–2019 and 2021). For subsurface soil  
 259 moisture, permanently installed soil moisture probes: SMT-100 at forest and grassland sites, and CS650 at  
 260 agroforestry and cropland sites. Measurements were recorded at 15-minute intervals with two replicates per depth.  
 261 To facilitate data processing and consistency, all soil moisture datasets were aggregated into daily mean values,  
 262 resulting in one volumetric water content value per site and soil depth. Details of the measurement devices, depth  
 263 intervals, and aggregation methods is summarized in Table S2. Daily precipitation samples for stable water isotope  
 264 analysis from June 2018 onward were collected at the Hasenfelde AWS, and earlier data were obtained from the  
 265 Berlin weather station. Soil water isotopes were sampled from bulk soil at the four plot sites at five depths (0–5,  
 266 5–10, 10–20, 20–30, and 30–50 cm) every 3–4 weeks during the growing season. The isotope data were  
 267 aggregated according to the thickness of the corresponding model soil compartments. All isotope values are  
 268 reported relative to Vienna Standard Mean Ocean Water (VSMOW). Further details on site instrumentation and  
 269 data collection are described in Landgraf et al. (2022).

270 **Table 2.** Summary of the used climate, vegetation, soil moisture, and isotope data.

Data	Unit	Period	Timestep	Acquisition
<i>Climate data</i>				
Precipitation	mm/d	2000-2024	Daily	Muencheberg weather station (52.52°, 14.12 °)
Temperature	°C			
Windspeed	m/s			
Relative humidity	%		Hourly	ERA5
Net shortwave radiation	W/m <sup>2</sup>			
Net longwave radiation				
Potential evapotranspiration	mm/d	Daily	FAO Penman-Monteith equation	
<i>Vegetation data</i>				
Leaf area index	-	2000-2024	8-days	MODIS at broadleaf forest, coniferous, and agroforestry sites
<i>Soil data</i>				
Soil moisture	%	2018-2024	Daily	broadleaf forest, cropland, agroforestry, and grassland sites
<i>Isotope data</i>				
Precipitation isotope $\delta^2\text{H}$	‰	2000-2024	Daily	Hasenfelde (52.41°N, 14.19°E), weather station in Berlin
Soil water isotope		2018-2019, 2021	Daily	Manually at broadleaf forest, cropland, agroforestry, and grassland sites

271

### 272 3.4 Model Calibration and Validation

273 The EcoPlot-iso model was calibrated using the Monte Carlo approach combined with a multi-criteria evaluation  
274 based on soil moisture and soil water isotope observations at each land use site. For each calibration, 100,000  
275 parameter sets were generated using the Latin Hypercube Sampling (LHS) within a Monte Carlo framework  
276 (McKay et al., 1979) to broadly sample the parameter space and capture a wide range of plausible model behaviors.

277 The initial parameter ranges were defined based on a literature values and site-specific knowledge. Specifically,  
278 initial ranges for the radiation extinction factor ( $rE$ ) were guided by vegetation-specific light attenuation  
279 coefficients from canopy gap-fraction theory (Larcher, 1975; Gigante et al., 2009), using typical reference values  
280 of 0.35 for grasslands, 0.45 for croplands, and 0.65 for forests. Initial ranges for the interception storage capacity  
281 parameter ( $\alpha$ ) were guided by scaling values reported in global syntheses of canopy interception storage (Zhong  
282 et al., 2022) and interception sensitivity studies (Barnard et al., 2014), accounting for differences in model time  
283 step and formulation. The resulting interception evaporation is consistent with observational studies indicating  
284 that canopy interception losses typically represent approximately 10–30% of annual precipitation in forested  
285 systems (Staelens et al., 2008; Llorens & Domingo, 2007).

286 Model performance was evaluated using the modified Kling-Gupta Efficiency ( $mKGE$ ) (Kling et al., 2012),  
287 calculated separately for soil moisture ( $mKGE_{sm}$ ) and soil water isotopes ( $mKGE_{iso}$ ) at each of the three soil depth  
288 layers. Calibration followed a two-step refinement process. In the first step, based on the initial parameter ranges,  
289 parameter sets were retained only if they fell within the intersection of the top 60th percentile of all six individual  
290  $mKGE$  metrics (i.e. soil moisture and soil water isotopes at each of the three soil depths). This intersection-based  
291 filtering ensured that retained simulations performed consistently well across all evaluated variables and depths.  
292 By retaining only the performance metrics and corresponding parameter sets, this step efficiently screened the  
293 parameter space while substantially reducing data storage requirements during the initial exploration.

294 In the second step, the model was re-run using the retained parameter space obtained from Step 1. For these re-  
295 run simulations, an average  $mKGE$  value across depths and variables was then used as the objective performance  
296 metric (Eq. 5), and the 100 best-performing simulations were selected for final analysis. The model parameters,  
297 their initial ranges, and the refined ranges for each of land use are summarized in Table S3 in the Supplement. To  
298 assess parameter constraints and equifinality, the probability density distributions and median values of the  
299 calibrated parameters were derived from the 100 best-performing simulations for each site (see Fig. S4). These  
300 were then used to evaluate the convergence of the parameters relative to their initial ranges.

$$301 \quad mKGE = \frac{\sum_i^3 mKGE_{sm} + \sum_i^3 mKGE_{iso}}{6} \quad (5)$$

302 Model parameters were calibrated using the full available observation, comprising seven years of soil moisture  
303 data and three years of soil water isotope data, in order to maximise information content under limited isotope  
304 availability (Shen et al., 2022). To additionally assess model robustness beyond a shorter calibration window, a  
305 split-sample calibration–validation experiment was conducted consistently across all land-use types. In this  
306 experiment, the model was calibrated using an earlier subset of the soil moisture and isotope observations,  
307 followed by validation against an independent soil moisture period, as isotope observations were not available for  
308 validation. Results from this split-sample evaluation, which showed good parameter transferability across most

309 sites, are reported in Table S4 and Figures S5–S7 of the Supplement. Given this transferability, the full-period  
310 calibration was retained for the main scenario simulations, as it provides more stable parameter estimates under  
311 data limitations, while the split-sample results are presented for transparency and robustness assessment.

### 312 **3.5 Development and Application of a Generic Forest Management Scenario Framework**

313 The primary goal of this study was to develop a new, parsimonious and generic forest management scenario  
314 framework to evaluate how forest type, forest density, and root distribution —associated with forest age—  
315 influence long-term water partitioning and ecohydrological resilience under comparable environmental conditions.  
316 This framework was designed to capture the dominant effects of vegetation structure—such as interception and  
317 transpiration through canopy and root networks—on water partitioning, rather than to reproduce detailed species-  
318 specific physiology.

319 Based on this conceptual framework, baseline simulations covering the period 2000-2024 were established using  
320 EcoPlot-iso model at three forest sites within the DMC (broadleaf forest, conifer forest, and agroforestry). These  
321 baseline simulations provide forest-type-specific reference conditions against which alternative management  
322 scenarios were evaluated.

323 To isolate the effects of forest management from site-specific soil properties and boundary conditions, we  
324 extended the observed forest-site configurations by systematically combining each forest-type-specific vegetation  
325 parameter with each site-specific soil parameter, resulting in a  $3 \times 3$  scenario matrix (Fig. 3). The diagonal entries  
326 represent the observed site-based reference configurations—namely, Broadleaf forest site, Conifer forest site, and  
327 Agroforestry site —and are therefore treated as baseline scenarios. The remaining cross-combinations represent  
328 hypothetical but plausible forest-site (soil) configurations, in which vegetation characteristics are applied to  
329 alternative site-specific soil hydraulic properties and boundary conditions (e.g., soil texture and compaction). This  
330 design enables vegetation effects to be assessed independently of site-specific controls, while explicitly  
331 acknowledging that soil hydraulic properties and boundary conditions remain inherently site-dependent.  
332 Ensemble-based comparisons across site configurations for each forest type therefore support a more robust and  
333 generic interpretation of ecohydrological behaviour.

334 Specifically, for each of forest-site baseline scenario calibration, we retained the top 100 best-performing  
335 simulations—ranked by average mKGE—and their corresponding parameter sets (as described in Section 3.4).  
336 Forest-type-specific vegetation parameters (e.g.,  $rE$ ,  $\alpha$ ) were derived from site-specific calibrations for broadleaf,  
337 conifer, and agroforestry systems, and their median values from the 100 best-performing simulations at each site  
338 were used to represent characteristic vegetation conditions. The root distribution parameter ( $\beta$ ) was not treated as  
339 strictly vegetation-specific, but as jointly influenced by vegetation type, soil properties, and soil water availability  
340 (Fig. S4). These calibrated parameter sets were then used for subsequent scenario simulations to ensure physically  
341 consistent parameter configurations across all forest types. In contrast, soil-related parameters (e.g.,  $ks1$ ,  $ks2$ ,  $ks3$ ,  
342  $S_{max}$ ,  $GW_{max}$ ,  $L_{max}$ ) were retained from the corresponding forest sites to preserve site-specific hydraulic  
343 properties and boundary conditions.

344 For vegetation forcing, we used forest-type-specific observed LAI time series (broadleaf, coniferous, and  
345 agroforestry), derived from the MODIS LAI products, described in Section 3.3 (Table 2; Fig. S3d). Forest-type-  
346 specific initial soil moisture conditions for the three soil layers were kept consistent with the corresponding

347 baseline simulations. All scenario simulations were driven using identical climate input data, precipitation isotope  
348 time series, and potential evapotranspiration forcing as the baseline simulations to isolate the effects of forest  
349 characteristics and management.

350 The scenario framework varied three key dimensions of forest management:

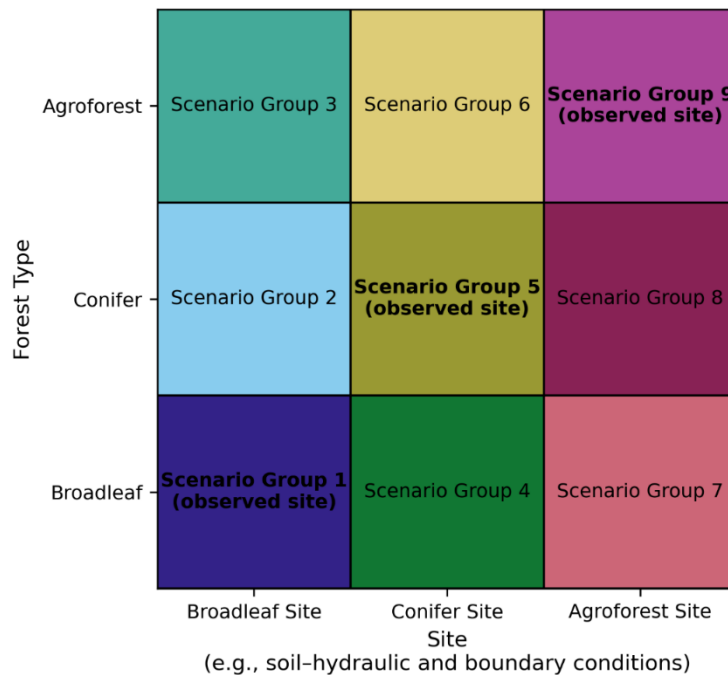
- 351 a) Forest type was varied by implementing three canopy types—broadleaf, conifer, and agroforestry—each  
352 assigned type-specific LAI time series to reflect differences in canopy structure.
- 353 b) Forest density was varied by multiplying the reference LAI by a scaling factor ranging from 0.2 to 1.8.  
354 Higher forest density was represented by scaling factors  $>1.0$ , indicating denser canopy cover, while  
355 lower forest density corresponded to factors  $<1.0$ , reflecting more open canopy conditions. The applied  
356 LAI scaling range (0.2–1.8) follows previous tracer-aided modelling approaches (Neill et al., 2021) and  
357 spans realistic management-induced variability in canopy density, while remaining consistent with  
358 reported LAI values for mature European forests (Leuschner et al., 2006).
- 359 c) Root water uptake efficiency was varied by scaling the site-calibrated  $\beta$  parameter to represent  
360 contrasting vertical root distributions associated with forest developmental stage. Three rooting scenarios  
361 were considered:  $0.5 \times \beta$ ,  $1.0 \times \beta$ , and  $2.0 \times \beta$ , where  $\beta$  is the calibrated value for each forest site. Lower  
362 scaled values ( $0.5 \times \beta$ ) represent more developed forests with deeper, less surface-weighted rooting  
363 systems, while higher scaled values ( $2.0 \times \beta$ ) represent younger or less-developed forests with shallower,  
364 more surface-weighted rooting distributions (see Fig. S1). The  $1.0 \times \beta$  scenario corresponds to the  
365 observed rooting distribution at each forest site.

366 Within this framework, LAI and rooting distribution were treated as independent scenario dimensions. LAI scaling  
367 represented management-induced changes in canopy density, whereas rooting distribution scenarios reflected  
368 contrasts in belowground water uptake. Their combined effects on water fluxes were evaluated without assuming  
369 a fixed linkage between canopy structure and rooting depth. This separation acknowledges that canopy density  
370 can change rapidly through management (e.g., thinning or harvesting), while rooting characteristics typically  
371 reflect longer-term stand development, thereby allowing realistic representation of above- and belowground  
372 controls on water partitioning.

373 Although EcoPlot-iso was originally developed for plot-scale applications, it is applied here to represent  
374 ecohydrological fluxes in a range of well-characterized sites within the DMC region. The model employs a one-  
375 dimensional approach that does not explicitly account for lateral fluxes; however, this simplification is intentional.  
376 It enables clearer interpretation of process-level dynamics under contrasting vegetation and climate conditions,  
377 making it suitable for general scenario analysis. This assumption is especially justified in the DMC catchment,  
378 which is characterized by flat, lowland topography and is predominantly governed by vertical hydrological fluxes  
379 (Kleine et al., 2021; Smith et al., 2020).

380 The framework is not intended to reproduce exact spatial patterns or detailed species-specific physiology, but  
381 rather to capture the dominant effects of vegetation structure on vertical water fluxes and soil moisture dynamics.  
382 By focusing on variations in forest type, forest density, and root distribution associated with forest age and  
383 management, the framework enables a generalized assessment of long-term water partitioning and  
384 ecohydrological resilience under comparable environmental conditions. As such, it provides a practical and

385 transferable tool for evaluating forest management impacts on water availability and ecohydrological resilience  
 386 in drought-sensitive lowland catchments.



387

388 **Figure 3.** Matrix of nine Scenario Groups formed by combining three site-specific configurations (Broadleaf Site,  
 389 Conifer Site, and Agroforest Site) with three forest types (Broadleaf, Conifer, and Agroforest). Each colored block  
 390 represents a Scenario Group consisting of multiple sub-scenarios (e.g., varying forest densities and root water  
 391 uptake distributions). Diagonal entries (Scenario Groups 1, 5, and 9), marked as “observed configuration”,  
 392 correspond to forest–site combinations observed at the field sites, where vegetation type and site-specific soil–  
 393 hydraulic and boundary conditions are consistent with real-world conditions.

## 394 4 Results

### 395 4.1 Dynamics of Soil Moisture and Soil Water Isotopes at the Broadleaf Forest Site

396 Figure 4 shows the 25-year baseline simulations of soil moisture and soil water isotopes dynamics at the broadleaf  
 397 forest site at a daily time step as an example. In general, the model effectively captures the magnitude, variability,  
 398 extremes, and timing of soil moisture dynamics. Surface soil moisture shows higher variability than deeper layers.  
 399 Based on the Kling-Gupta Efficiency (KGE), soil moisture simulations generally perform better in the deep layer  
 400 than in the shallow and lower layers, though this may partly reflect the more limited variance in deeper soil  
 401 moisture. In addition, the model slightly overestimates low soil moisture in the deeper layers during wet summers  
 402 (e.g., 2023, 2024) and underestimates soil moisture during dry winters (e.g., 2021 and 2022). Soil water isotope  
 403 simulations also perform well, with higher KGE values in the intermediate layer than in surface and deeper layers.  
 404 The uncertainty range of soil water isotope simulations is narrower than that of soil moisture, indicating lower  
 405 uncertainty in the isotope predictions.

406 Table 3 shows the Kling-Gupta Efficiency (KGE) and Root Mean Square Error (RMSE) values for soil moisture  
 407 and soil water isotopes across different land use plots. In all other cases the KGEs for soil moisture are similar to  
 408 the broadleaved plot, and soil water isotopes are reasonably reproduced, indicating the model’s robustness and

409 transferability. These results provide strong support for the appropriateness of applying EcoPlot-iso to assess the  
 410 impacts of alternative forest management scenarios in subsequent analyses. In addition, simulated  
 411 evapotranspiration was independently evaluated against MODIS-derived ET for all land use types, with model  
 412 performance quantified using RMSE and KGE metrics (Table S4). This independent evaluation provides further  
 413 support for the model’s ability to reproduce key water fluxes beyond the variables used for calibration.

414 **Table 3.** Model performance metrics for soil moisture and soil water isotopes ( $\delta^2\text{H}$ ) at each land use site over the  
 415 full evaluation period (2000–2024), evaluated using the Kling–Gupta Efficiency (KGE) and the root mean square  
 416 error (RMSE, mm for soil moisture and ‰ for  $\delta^2\text{H}$ ). Metrics are computed by comparing observed and simulated  
 417 time series at each soil depth.

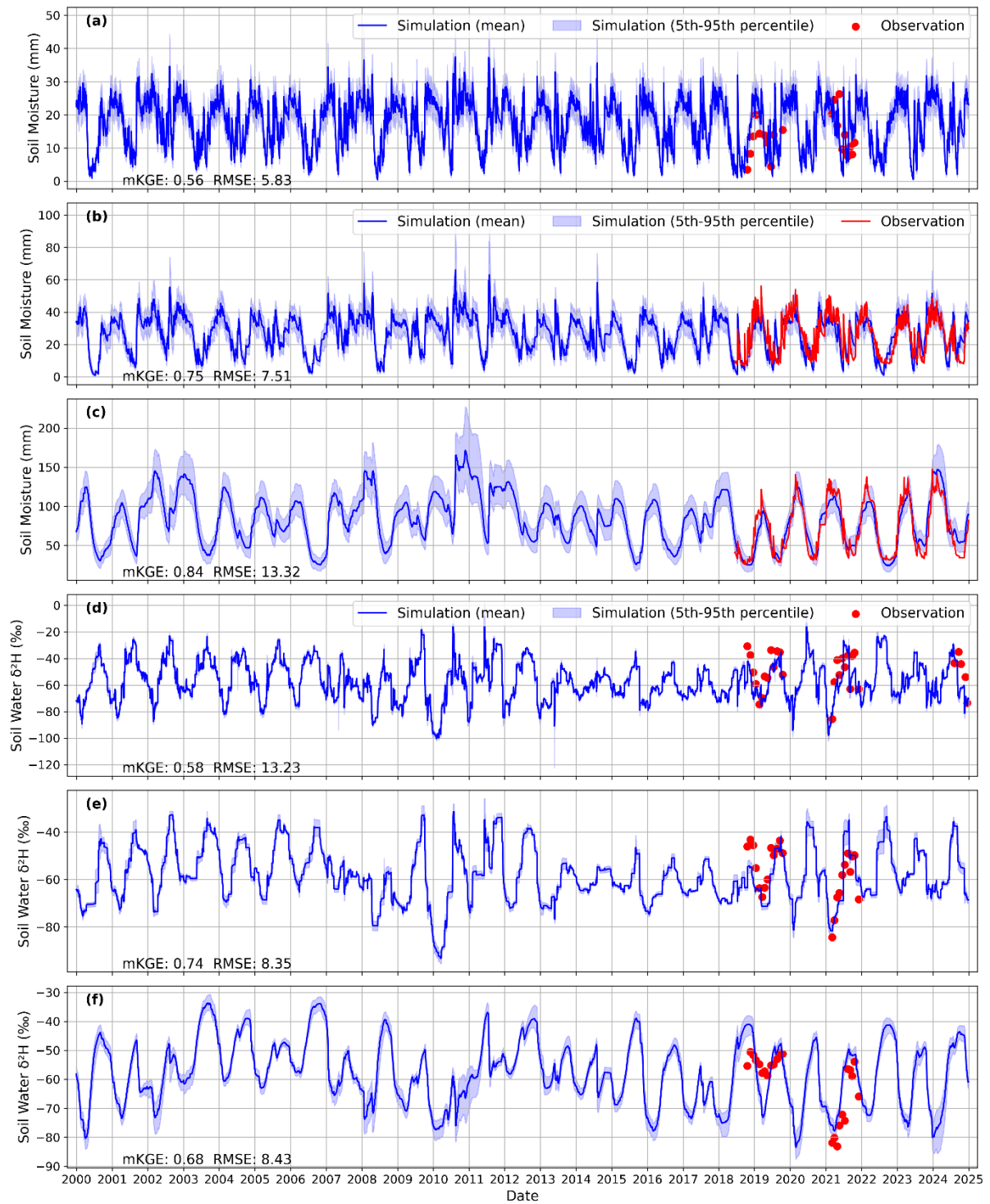
Sites	Soil moisture						Soil water isotope ( $\delta^2\text{H}$ )					
	Upper		Lower		Deep		Upper		Lower		Deep	
	KGE	RMSE	KGE	RMSE	KGE	RMSE	KGE	RMSE	KGE	RMSE	KGE	RMSE
Broadleaf Forest	0.56	5.83	0.75	7.51	0.84	13.32	0.58	13.23	0.74	8.35	0.68	8.43
Conifer forest	0.61	5.77	0.68	8.68	0.70	5.56	0.67	11.69	0.80	6.94	0.50	13.09
Agroforestry	0.72	5.22	0.79	6.63	0.77	23.43	0.82	8.09	0.85	10.45	0.79	8.98
Grassland	0.89	1.67	0.71	6.18	0.72	16.01	0.71	9.07	0.77	7.69	0.61	8.36
Cropland	0.53	5.84	0.62	8.88	0.71	22.36	0.83	8.36	0.85	9.19	0.36	13.71

418

419

420

421



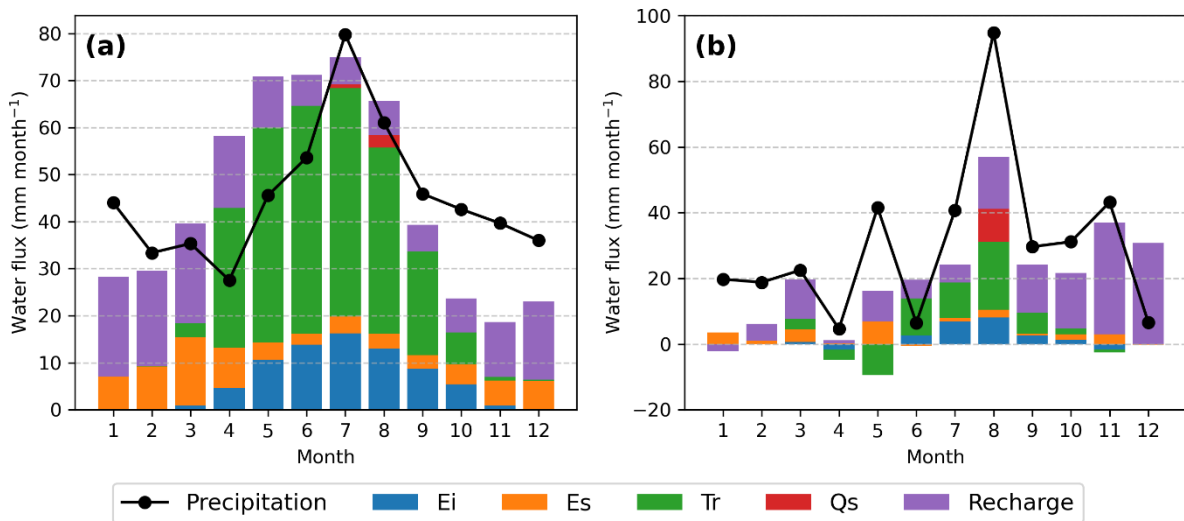
422  
 423  
 424  
 425  
 426  
 427  
 428  
 429

**Figure 4.** Long-term (2000–2024) simulations of soil moisture and soil water isotope ( $\delta^2\text{H}$ ) at three different depths using EcoPlot-iso at a broadleaf forest site in the Demnitzer Millcreek catchment. (a–c) Simulated (mean  $\pm$  5th–95th percentile) and observed soil moisture at surface (0–10 cm), lower (20–30 cm), and deeper (30–100 cm) layers. (d–f) Simulated (mean  $\pm$  5th–95th percentile) and observed soil water isotopic composition ( $\delta^2\text{H}$ ) at corresponding depths. The blue line represents the mean value of the 100 best simulations, while the shaded area indicates the range between the 5th and 95th percentiles of these simulations. The red points and red line represent observed values. Kling-Gupta Efficiency (KGE) values for each simulation are indicated in the respective panels.

430 **4.2 Water Balance Components Under Different Wetness Conditions at the Broadleaf Forest Site**

431 Figure 5 presents the mean monthly water balance components and their changes between dry and wet years for  
 432 the baseline simulation at the broadleaved forest site from 2000 to 2024. Groundwater recharge dominates blue  
 433 water fluxes, while surface runoff is rare and occurs only during extreme summer rainfall events (Fig. 5a).  
 434 Transpiration and canopy evaporation dominate in summer, while soil evaporation peaks in spring. Across dry  
 435 and wet years, groundwater recharge shows the strongest sensitivity to interannual wetness, with reduced recharge  
 436 during dry years and enhanced recharge during wet years following precipitation anomalies (Figs. 5b and S1). In  
 437 contrast, transpiration remains relatively stable despite differences in annual wetness, indicating resilient  
 438 vegetation function. This stability likely reflects the mature age of the forest (~60 years), although gradual changes  
 439 in forest structure over the 20-year period may also play a role. Corresponding water balance results for the conifer  
 440 forest and agroforestry sites are provided in the Supplementary Material (Fig. S9). Across the three forest types,  
 441 the conifer forest exhibits the largest changes in groundwater recharge between dry and wet years, particularly in  
 442 August, whereas agroforestry shows comparatively smaller changes than the broadleaf forest, indicating higher  
 443 ecohydrological resilience. Overall, these seasonal patterns offer key insights into water partitioning under three  
 444 forest baseline conditions and establish an important baseline for evaluating the impacts of alternative forest  
 445 management scenarios.

446



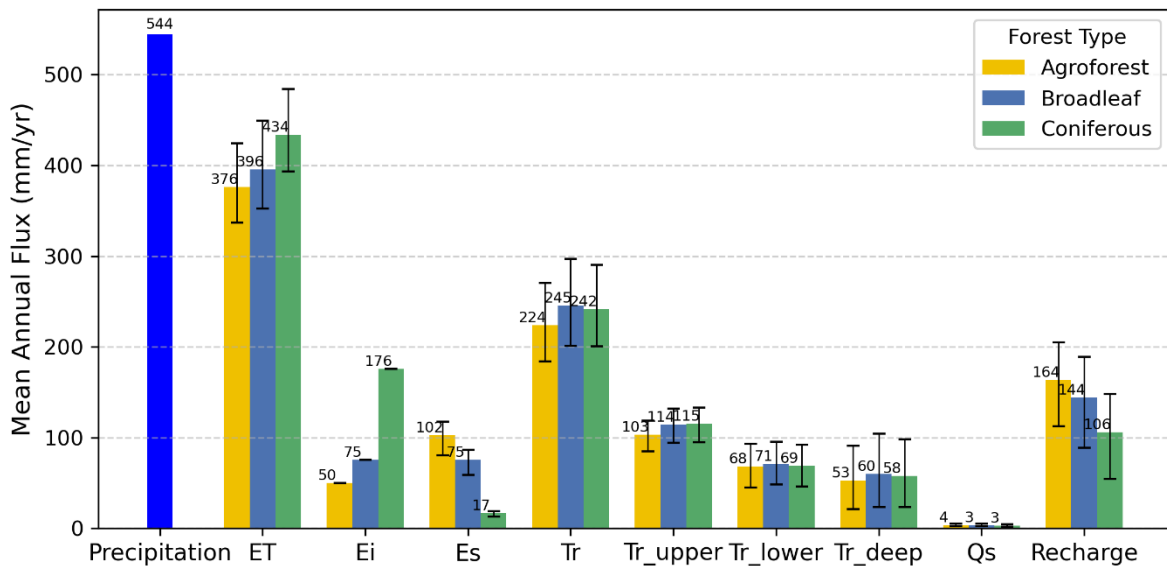
447 **Figure 5.** Mean monthly water balance components for the broadleaf forest site in the Demnitzer Millcreek  
 448 catchment over 2000–2024, simulated with EcoPlot-iso using the mean of the best 100 parameter sets (see Section  
 449 3.4 for details). Stacked bars show monthly totals of interception evaporation (Ei), soil evaporation (Es),  
 450 transpiration (Tr), surface runoff (Qs), and groundwater recharge, while the black line indicates precipitation (P).  
 451 (a) Long-term mean monthly water balance (mm month<sup>-1</sup>). (b) Differences between wet years (2002, 2007, 2010,  
 452 2023) and dry years (2006, 2018, 2022), expressed as wet minus dry (mm month<sup>-1</sup>).  
 453  
 454

455 **4.3 Impacts of Forest Management on Water Partitioning and Soil Moisture**

456 Results in this section are based on the full forest management scenario framework, including all nine forest–site  
 457 Scenario Groups and their associated ensemble simulations (Fig. 3), rather than on the observed baseline  
 458 configurations alone.

459 **4.3.1 Water Balance and Partitioning Across Forest Types**

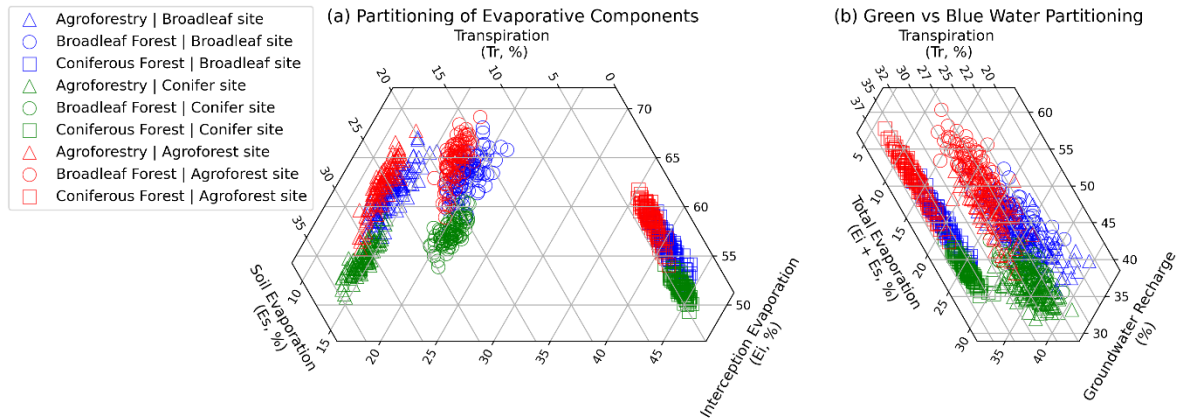
460 Figure 6 compares the mean annual water balance components across broadleaf forest, coniferous forest, and  
 461 agroforestry types based on the ensemble mean of simulations derived from the paired vegetation–site soil  
 462 parameter configurations (Fig. 3), under reference canopy and rooting conditions ( $LAI\ scaling = 1; \beta = 1 \times \beta$ ).  
 463 Results showed that evapotranspiration under coniferous forests accounted for 7% more of annual precipitation  
 464 than broadleaf forest, and 11% more than in agroforestry systems. This was primarily due to higher transpiration  
 465 ( $Tr$ ) and canopy interception evaporation ( $Ei$ ). In contrast, soil evaporation ( $Es$ ) and groundwater recharge  
 466 ( $Recharge$ ) were lowest in conifers and highest in agroforestry. Agroforestry had 11% more groundwater recharge  
 467 relative to annual precipitation than conifers, and 4% more than broadleaf forests. Across forest types, the largest  
 468 fraction of transpiration originated from the upper soil layer ( $Tr\_Upper$ ), reflecting its closer coupling to  
 469 precipitation inputs and higher soil moisture availability, while surface runoff ( $Qs$ ) remained minimal and nearly  
 470 identical. These results reflect the influence of forest structure and canopy cover on ecohydrological partitioning,  
 471 with coniferous systems favoring atmospheric losses and agroforestry promoting soil evaporation and subsurface  
 472 recharge. They underscore the trade-offs between evapotranspiration and groundwater recharge across different  
 473 forest types.



474 **Figure 6.** Comparison of mean annual water balance components across different forest types: broadleaf (blue),  
 475 coniferous (green), and agroforestry (yellow). Bars represent the mean annual flux based on 25-year totals, with  
 476 error bars indicating the 5th and 95th percentile ranges of the 100 best simulations. All simulations were conducted  
 477 under baseline conditions with a fixed forest root parameter  $\beta$  of 0 and LAI scaling factor of 1.0.  
 478

479 Figure 7 presents ternary diagrams illustrating the relative partitioning of key water flux components across three  
 480 forest types based on individual simulations from the paired vegetation–site soil parameter configurations under  
 481 reference canopy and rooting conditions. Transpiration predominates in all three forest types (Fig. 7a). The conifer  
 482 forest exhibit a distinct pattern, characterized by the lowest soil evaporation ( $Es$ ) and the highest interception  
 483 evaporation ( $Ei$ ) partitioning compared to broadleaf forest and agroforestry systems (Fig. 7a). In terms of green–  
 484 blue water partitioning, the agroforestry system shows the largest groundwater recharge contribution (Fig. 7b).  
 485 Broadleaf and agroforestry forests display largely overlapping partitioning patterns overall, although interception  
 486 evaporation and total evaporation differ notably between the two (Fig. 7a–b). Differences in soil properties also

487 influence transpiration partitioning, following the order agroforestry site > broadleaf site > conifer site. The  
 488 conifer site is characterized by coarse sandy soil with lower water retention and faster drainage, whereas the  
 489 agroforestry site has greater water-holding capacity, which likely contributes to the observed differences in  
 490 transpiration.



491 **Figure 7.** Water flux partitioning illustrated using ternary diagrams based on individual model simulations derived  
 492 from the paired vegetation–site soil parameter configurations for three forest types: agroforestry, broadleaf forest,  
 493 and coniferous forest, under reference canopy and rooting conditions ( $LAI$  scaling = 1.0;  $\beta = 1 \times \beta$ ). (a) Partitioning  
 494 of total evapotranspiration into transpiration ( $Tr$ ), soil evaporation ( $Es$ ), and interception evaporation ( $Ei$ ). (b)  
 495 Partitioning of water fluxes into green water ( $Tr$  and  $E = Ei + Es$ ) and blue water (groundwater recharge). Each  
 496 point represents the normalized annual mean flux from a 25-year simulation. Colored markers denote different  
 497 forest types.  
 498

### 499 4.3.2 Annual Mean Water Flux Responses to Forest Management Scenarios

500 The annual mean responses of key ecohydrological fluxes to forest management scenarios across all paired  
 501 vegetation–site configurations are summarized in Fig. 8, while the detailed number and visualization of green and  
 502 blue water partitioning are provided in the Fig. S10 in Supplementary Material. Figure S10 presents heatmaps of  
 503 evapotranspiration ( $ET$ ), groundwater recharge (Recharge), transpiration ( $Tr$ ),  $ET$  partitioning ( $ET/P$ ),  
 504 groundwater recharge partitioning (Recharge/ $P$ ) and green water partitioning ( $Tr/ET$ ) for agroforests, broadleaf  
 505 forest, and coniferous forest scenarios.

506 Across all forest management scenarios, annual mean evapotranspiration ranges from 285 mm/yr to 454 mm/yr,  
 507 with  $ET$  fraction relative to precipitation varying between 0.52 and 0.84 (Fig. S10). In contrast, groundwater  
 508 recharge ranges from 85 mm/yr to 254 mm/yr, reflecting strong sensitivity to vegetation structure and canopy  
 509 density. Annual mean transpiration ( $Tr$ ) varies between 77 mm/yr and 261 mm/yr, with the corresponding green  
 510 water partitioning ( $Tr/ET$ ) ranging from 0.27 to 0.64. These results underscore the significant influence of  
 511 vegetation type and structure on ecohydrological fluxes and water partitioning outcomes.

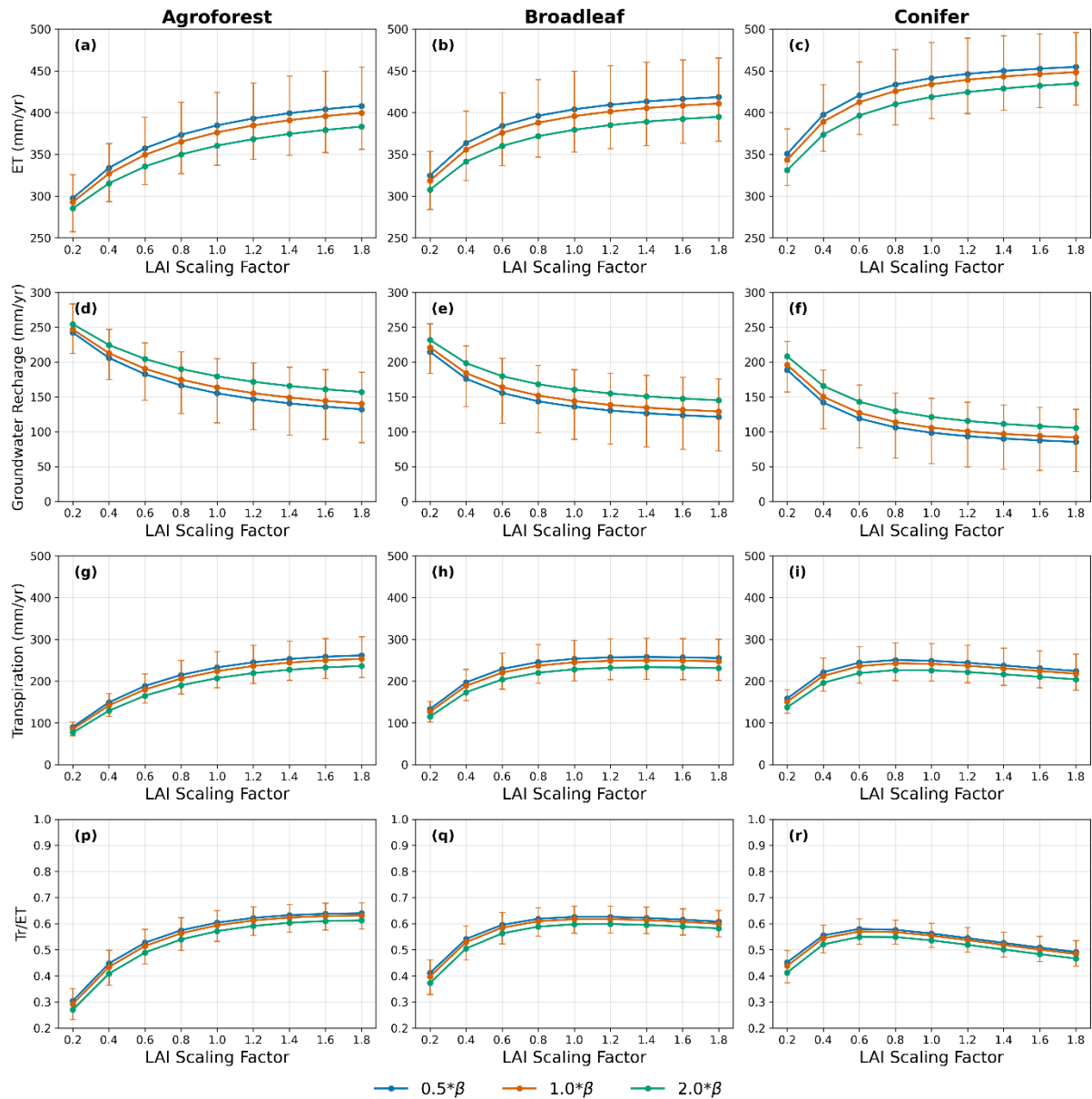
512 Consistent with these detailed patterns, Figure 8 shows that both transpiration and evapotranspiration increase  
 513 with higher  $LAI$  scaling factors, while groundwater recharge decreases. Figures 8a and 8b illustrate the trade-off  
 514 between increased  $ET$  and reduced groundwater recharge under different forest management scenarios.  
 515 Transpiration and  $ET$  rise rapidly at first, then slow down and transpiration even slightly decreases for conifer  
 516 forests due to soil moisture limitation (Fig. 8c). This decline is not observed in broadleaf or agroforestry systems,

517 likely due to their different seasonal LAI patterns. While summer LAI values for broadleaf and coniferous forests  
518 may be similar, the consistently high year-round LAI in conifers can exacerbate moisture stress.

519 At higher LAI levels, transpiration decreases slightly while canopy interception evaporation increase (Fig. S11).  
520 In dense coniferous stands, excessive interception and persistently dry soils limit root water uptake, reducing  
521 vegetation function. This highlights a trade-off between transpiration and interception evaporation. The resulting  
522 moisture limitation suggests that such high-density forests may not be sustainable under water-limited conditions,  
523 as this negative feedback could constrain long-term forest growth and persistence. In addition, forests with  
524 shallow-rooted trees—such as young stands —tend to transpire less, generate more groundwater recharge, and  
525 exhibit lower Tr/ET ratios compared to deep-rooted forests. However, even at constant LAI, transpiration declines  
526 with increasing canopy density, suggesting that rooting depth alone cannot compensate for moisture limitations  
527 in dense forests.

528

529



530  
531  
532  
533  
534  
535  
536

**Figure 8.** Annual mean ecohydrological fluxes for three forest types (Agroforest, Broadleaf, and Conifer) under varying LAI scaling factors and root depth scenarios, based on the ensemble mean of simulations derived from the paired vegetation–site soil parameter configurations (Figure 3). Panels (a)–(c) show evapotranspiration (ET), (d)–(f) show groundwater recharge, (g)–(i) show transpiration, and (p)–(r) show the ratio of transpiration to total evapotranspiration (Tr/ET). Lines represent different rooting depth scenarios ( $\beta$ ), while vertical bars denote the 5th–95th percentile range across ensemble simulations for the baseline rooting scenario ( $\beta = 1 \times \beta$ ).

### 537 4.3.3 Monthly Dynamics of Water Fluxes Responses to Forest Management Scenarios

538 Figure 9 shows monthly deviations in water balance components across forest management scenarios, based on  
539 the ensemble mean of simulations derived from the paired vegetation–site soil parameter configurations (Fig. 3)  
540 under reference canopy and rooting conditions (LAI scaling = 1;  $\beta = 1 \times \beta$ ). Relative differences among forest  
541 types indicate that agroforestry exhibit lower transpiration and canopy evaporation, but higher soil evaporation  
542 during summer compared to broadleaf forests (Fig. 9a). They are also associated with greater groundwater  
543 recharge from summer through the following winter. A shift from broadleaf to conifer forests is expected to have  
544 a greater impact on the water balance than the shift from agroforest to broadleaf (Fig. 9a and 9b). Compared to  
545 broadleaf forests, conifer forests exhibit higher simulated transpiration in March (Fig. 9b), driven by increased

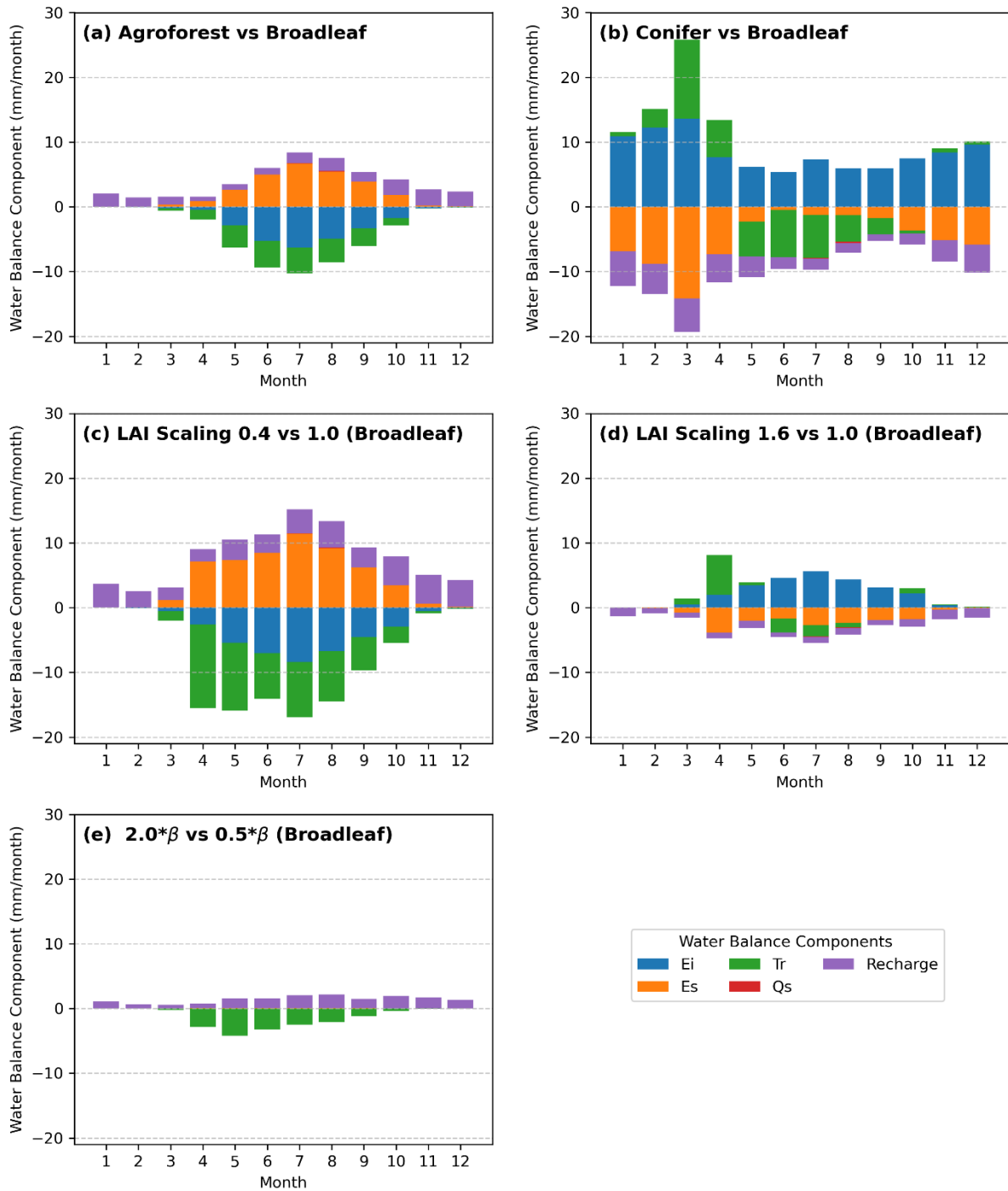
546 potential evapotranspiration and a relatively higher leaf area index (LAI) under wet soil conditions. This difference  
547 diminishes as the LAI of broadleaf forests increases in spring.

548 Changes in the LAI scaling factor influence water balance components in summer, increasing transpiration and  
549 canopy evaporation while reducing recharge and soil evaporation (Fig. 9c and 9d). Increasing the LAI scaling  
550 factor from 0.4 to 1.0 has a greater impact than reducing it from 1.6 to 1.0, as vegetation water use responds more  
551 sensitively at low LAI values but plateaus at higher values due to energy or soil moisture limitations. Altering the  
552 forest root parameter ( $\beta$ ), while using the same LAI time series, primarily affects deep-layer transpiration,  
553 reducing total transpiration and increasing recharge. Other water balance components remain unchanged because  
554 the LAI time series is held constant.

555 Figure 10 extends the monthly analysis by explicitly comparing water balance responses between wet and dry  
556 years across forest type, canopy density, and rooting scenarios. In contrast to Figure 9, which presents mean  
557 monthly deviations relative to reference conditions, Figure 10 highlights how these deviations differ under  
558 contrasting hydroclimatic conditions, thereby isolating drought-sensitivity effects.

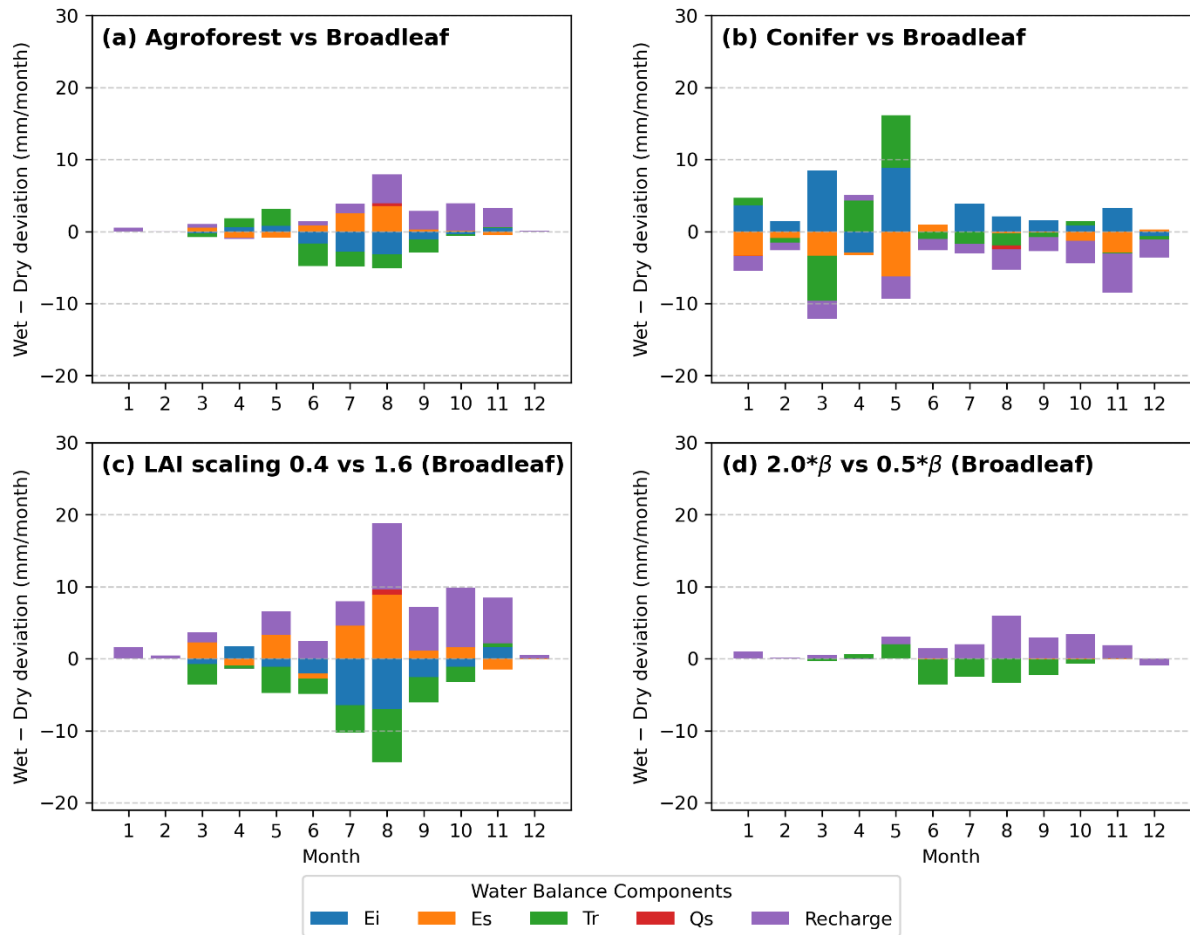
559 For agroforestry relative to broadleaf forests, hydroclimatic contrasts primarily affect groundwater recharge and  
560 transpiration, with the largest wet–dry differences occurring in late summer (Fig. 10a). This indicates a more  
561 buffered late-summer transpiration response in agroforestry systems under drought conditions. In contrast,  
562 differences between coniferous and broadleaf forests show the largest wet–dry contrasts in transpiration during  
563 May (Fig. 10b), rather than March as indicated by the mean monthly deviations in Figure 9b. This seasonal shift  
564 indicates that conifer transpiration is most drought-sensitive during the later spring period, likely reflecting  
565 sustained year-round transpiration and associated soil moisture drawdown in conifer forests, and highlighting  
566 differences in early growing-season water-use strategies between coniferous and broadleaf forests.

567 Figures 10c and 10d show that wet–dry differences are largest in summer (August), indicating that drought  
568 conditions amplify ecohydrological differences between low and high canopy density, as well as between shallow  
569 and deep root, particularly for transpiration and groundwater recharge. Overall, Figure 10 demonstrates that  
570 hydroclimatic extremes not only modify the magnitude of vegetation controls on water partitioning but also shift  
571 their seasonal expression, with important implications for ecohydrological resilience under future drought  
572 conditions.



573  
 574 **Figure 9.** Monthly deviations of water balance components relative to the baseline broadleaf forest scenario, based  
 575 on the ensemble mean of simulations derived from the paired vegetation–site soil parameter configurations (Fig.  
 576 3) under reference canopy and rooting conditions (LAI scaling = 1;  $\beta = 1 \times \beta$ ). Each panel illustrates the deviation  
 577 of monthly water balance components from the baseline simulation, with only one parameter modified in each  
 578 scenario: (a) Agroforest, (b) Conifer forest, (c) LAI scaling factor = 0.4, (d) LAI scaling factor = 1.6, and (e) Root  
 579 parameter  $\beta = 2.0$ . Tr: transpiration, Ei: canopy evaporation, Es: soil evaporation, Qs: surface runoff, Recharge:  
 580 groundwater recharge.

581



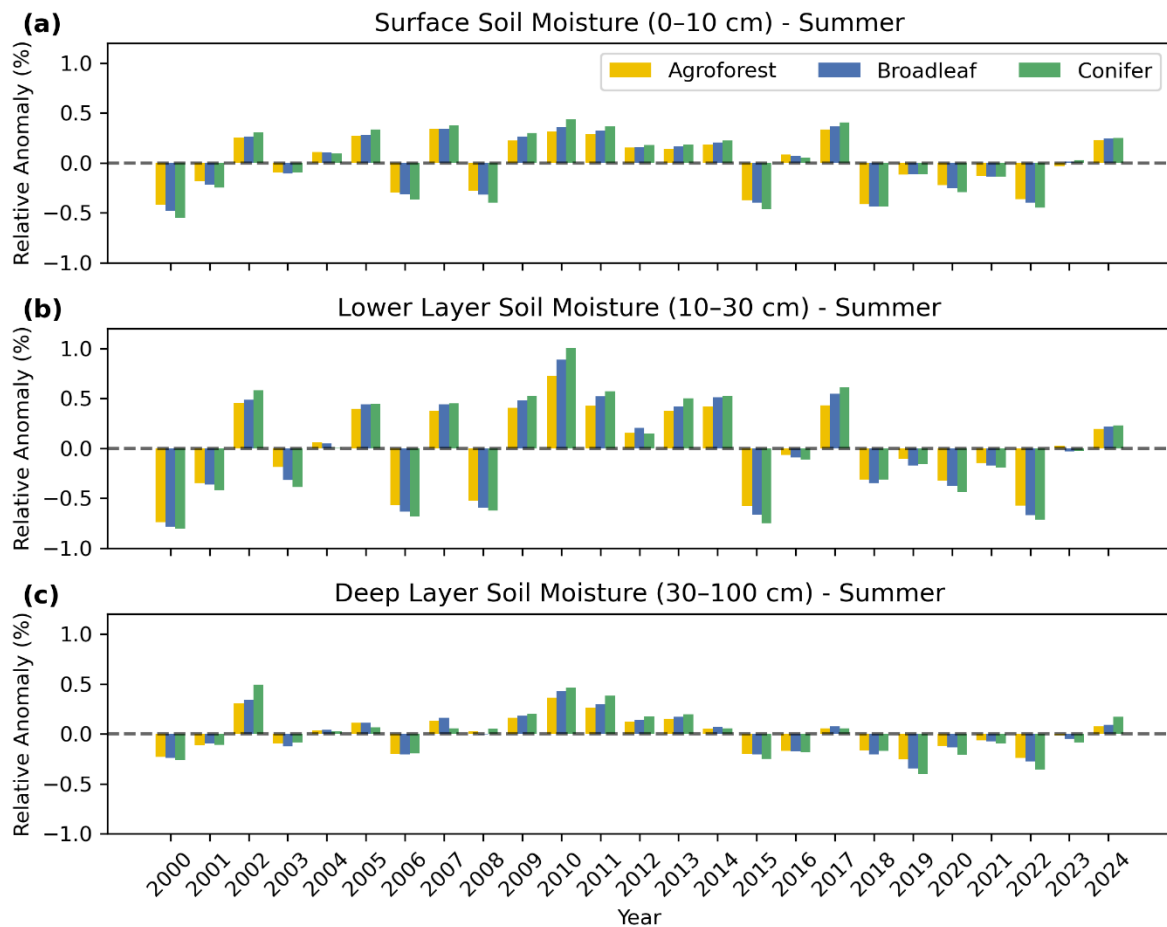
582

583 **Figure 10.** Monthly differences in water balance component deviations between wet and dry years across forest type, LAI scaling, and rooting ( $\beta$ ) scenarios. For each panel, values show the difference between wet-year and  
584 dry-year deviations of a given scenario relative to its reference scenario; positive (negative) values indicate  
585 stronger (weaker) contributions during wet years. Panels show: (a) Agroforest vs. Broadleaf; (b) Conifer vs.  
586 Broadleaf; (c) LAI scaling 0.4 vs. 1.6 for Broadleaf; (e)  $2.0 \times \beta$  vs.  $0.5 \times \beta$  for Broadleaf. Stacked bars indicate  
587 contributions from interception evaporation ( $E_i$ ), soil evaporation ( $E_s$ ), transpiration ( $T_r$ ), surface runoff ( $Q_s$ ), and  
588 groundwater recharge (Recharge). Wet years are 2002, 2007, 2010, and 2023; dry years are 2006, 2018, and 2022.  
589

#### 590 4.3.4 Soil Moisture Anomalies

591 Figure 11 shows the relative summer soil moisture anomalies across three forest types and three soil layers.  
592 Anomalies are calculated as the percentage deviation from the long-term seasonal mean, enabling normalized  
593 comparison across forest types and soil layers. Conifer forests exhibit the strongest soil moisture anomalies,  
594 followed by broadleaf forests, while agroforests exhibit the least variability, indicating greater stability in soil  
595 moisture. Furthermore, among the three soil layers, the intermediate layer (10–30 cm) consistently shows stronger  
596 anomalies across all forest types, with magnitudes nearly double those of the other layers, highlighting its  
597 vulnerability during summer drought. In contrast, the surface layer (0–10 cm) and deep layer (30–100 cm) exhibit  
598 weaker anomalies, likely due to frequent soil moisture replenishment by summer rainfall in the surface layer and  
599 either more stable moisture retention or greater water storage capacity at depth that compensates for drought  
600 impacts. Negative soil moisture anomalies are more pronounced in summer than in spring, reflecting the stronger  
601 seasonal drought effects and fluctuations in soil moisture (see Fig. S12). During spring, broadleaf forests and

602 agroforests display similar negative soil moisture anomalies, suggesting comparable seasonal soil moisture  
 603 dynamics between these forest types.



604  
 605 **Figure 11.** Relative summer (June–August) soil moisture anomalies across three soil layers: (a) surface (0–10  
 606 cm), (b) lower layer (10–30 cm), and (c) deep layer (30–100 cm) for three forest types (Agroforest, Broadleaf,  
 607 Conifer). Results are based on the ensemble mean of simulations derived from the paired vegetation–site soil  
 608 parameter configurations (Fig. 3) under reference canopy and rooting conditions (LAI scaling = 1;  $\beta = 1 \times \beta$ ).  
 609 Bars represent deviations from the long-term mean, with positive values indicating wetter conditions and negative  
 610 values indicating drier conditions.

## 611 5 Discussion

### 612 5.1 Vegetation Controls on Water Partitioning under Contrasting Forest Management Scenarios

613 Assessing the influence of different land use types on water availability is inherently challenging because of the  
 614 complex interactions among vegetation, climate, and soil properties (te Wierik et al., 2021; Zhang et al., 2001).  
 615 Different vegetation types have distinct water demands, and their contrasting canopy structures affect how  
 616 precipitation is intercepted and partitioned into infiltration, runoff, groundwater recharge, and evapotranspiration  
 617 (Brauman et al., 2010). Vegetation management practices can substantially alter these processes. Moreover, the  
 618 effects of vegetation and canopy structure may vary depending on underlying soil characteristics (Geris et al.,  
 619 2015). This complexity poses a significant challenge for land managers and policymakers, particularly in drought-  
 620 sensitive regions experiencing increasing aridity under climate change (Orth & Destouni, 2018). In such contexts,

621 providing informed guidance on sustainable land cover choices is increasingly important for maintaining long-  
622 term water availability (Estrela & Vargas, 2012). In regions where forestry has traditionally been a dominant land  
623 use, shifting hydroclimatic conditions underscore the need to assess the resilience of different forest types and  
624 management practices (Quandt et al., 2023). This requires evaluating water yield across multiple temporal scales,  
625 including the effects of forest management on annual and monthly water partitioning, and their implications for  
626 residual water availability—specifically streamflow generation and groundwater recharge during low-flow  
627 periods (Brown et al., 2005; Neill et al., 2021).

628 Although complex, process-based ecohydrological models such as RHESSys and EcH<sub>2</sub>O are well suited to  
629 capturing detailed interactions among hydrological processes and water fluxes in data-rich research settings, their  
630 broader application in forest and land management is often constrained by the availability of observation data  
631 required for model forcing and calibration, as well as computational demand (Fatichi et al., 2012; Kuppel et al.,  
632 2018; Tague & Band, 2004). In this study, we therefore adopt a parsimonious, tracer-aided, conceptual process-  
633 based modelling approach. This was not to replace more complex models, but to provide robust and management-  
634 relevant insights into the dominant vegetation-structural controls governing water partitioning under different  
635 forest management scenarios. This focus is particularly relevant for Brandenburg, northeastern Germany, where  
636 recent droughts have highlighted the vulnerability of traditional forest management practices dominated by Scots  
637 pine plantations (Luo et al., 2024). By employing the tracer-aided ecohydrological model EcoPlot-iso, we  
638 developed and applied a generic framework to quantify the long-term effects of variations in forest type, forest  
639 density and root distribution on both blue and green water fluxes. The framework is based on idealized  
640 monoculture forest scenarios and explicitly acknowledges that additional species-specific and process-level  
641 dynamics (e.g., stomatal regulation, VPD sensitivity, drought stress strategies) are not represented and remain  
642 important directions for future model development. While this study focused on idealized, homogeneous  
643 vegetation scenarios (broadleaf, conifer, and agroforestry) for clarity and comparability, EcoPlot-iso can be  
644 extended to simulate mixed-species stands, as its ecohydrological parameters are calibrated at the plot scale using  
645 a Monte Carlo approach, making it suitable for regions where diverse forest compositions are the norm. The  
646 applied LAI scaling range represents an intentionally broad, management-relevant envelope for exploring canopy  
647 density effects, and scenario results should therefore be interpreted in a relative rather than prescriptive sense.

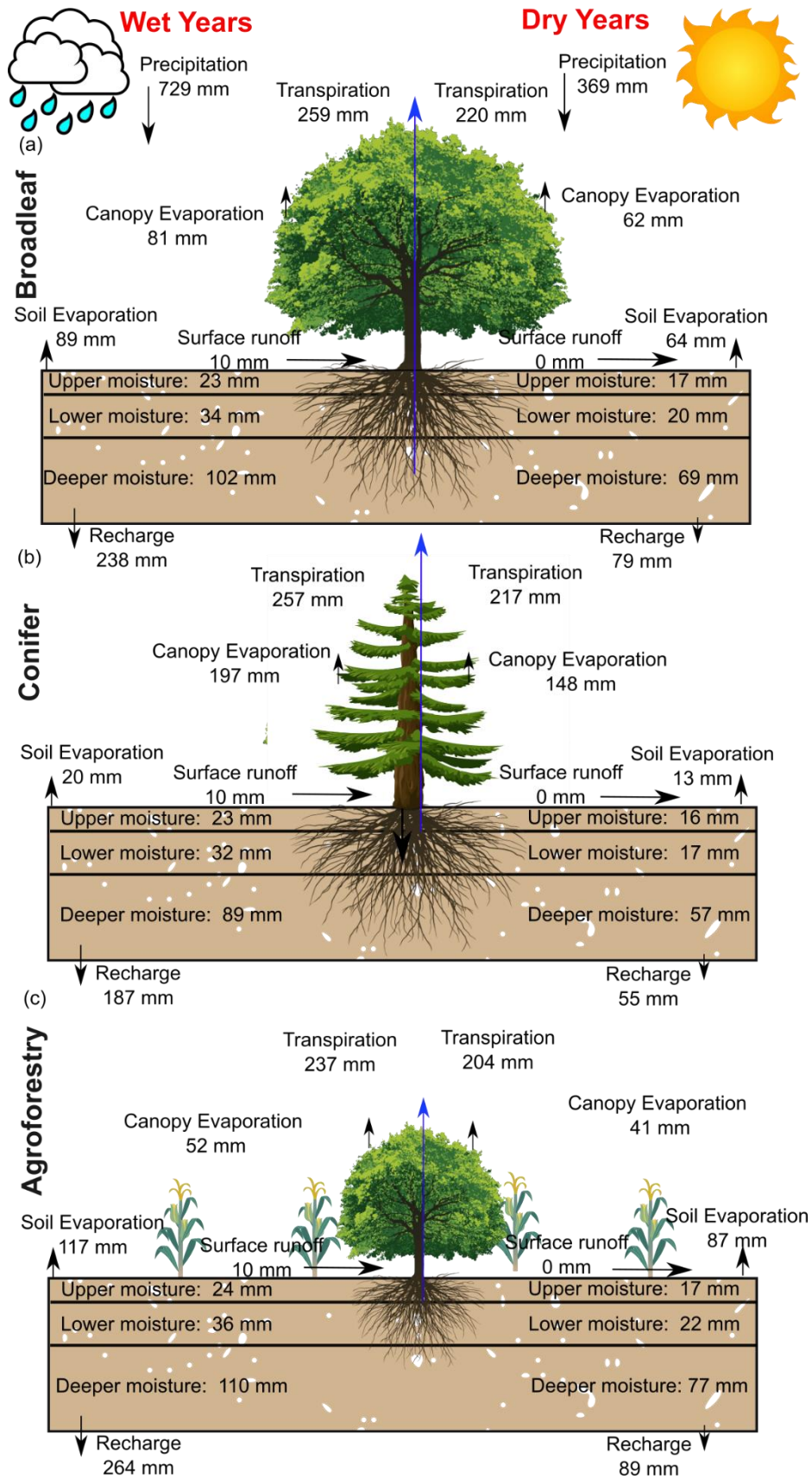
648 We acknowledge that the calibration of EcoPlot-iso is subject to parameter equifinality, whereby multiple  
649 parameter combinations can reproduce the observed soil moisture and isotope dynamics with similarly good  
650 performance. Rather than seeking a single optimal parameter set, our calibration strategy explicitly accounts for  
651 this equifinality by propagating uncertainty from the 100 best-performing simulations into all key results.  
652 Uncertainty envelopes (5th–95th percentiles) shown in Figures 4, 6, and 8 illustrate the range of annual and  
653 seasonal flux responses, enabling the magnitude of parametric uncertainty to be evaluated relative to differences  
654 among forest types and management scenarios. Although parametric uncertainty is non-negligible and in some  
655 cases comparable to different forest management scenarios, the main findings are supported by consistent  
656 ensemble-mean responses and clear directional differences in water partitioning across scenarios. Accordingly,  
657 results are interpreted in a relative and comparative sense, emphasizing management-relevant trade-offs rather  
658 than absolute flux predictions.

659 In the baseline simulations for broadleaf forest, conifer forest and agroforestry at the DMC site, the estimated  
660 mean annual evapotranspiration (ET) over 2000–2024 was 396, 434, and 376 mm yr<sup>-1</sup>, respectively, accounting  
661 for approximately 73%, 80%, and 69% of annual precipitation. These values are consistent with previous  
662 modelling studies at the DMC, which reported ET fractions ranging from 68% to over 80% of annual precipitation  
663 (Smith et al., 2021; Landgraf et al., 2023). Difference among studies may reflect interannual climate variability  
664 and the influence of particularly dry or wet years that are not captured by short-term assessments. Differences in  
665 model structure, parameterization, and input data may also contribute to the spread in reported ET values. In  
666 addition, to further assess model performance using an independent data source, simulated ET was evaluated  
667 against MODIS-derived ET for all land use sites in the DMC, including broadleaf forest, conifer forest,  
668 agroforestry, cropland, and grassland (Fig. S8 and Table S4). Model performance was quantified using KGE  
669 metrics calculated from daily ET, providing an external validation independent of the calibration data. While  
670 EcoPlot-iso tends to slightly underestimate ET relative to MODIS observations, KGE values indicate good  
671 agreement in temporal dynamics across land-use types, supporting the model’s ability to reproduce key ET  
672 variability. Overall, this evaluation underscores the importance of long-term simulations and independent data-  
673 based validation for capturing representative ecohydrological behavior and for assessing the impacts of forest  
674 management strategies under variable climatic conditions.

675 In catchments like DMC, where evapotranspiration (ET) is high, atmospheric demand is the primary driver of root  
676 water uptake, though vegetation plays a key role in regulating its impact on water availability. In Brandenburg,  
677 coniferous forests have traditionally been favored on sandy soils, but modelling indicates high water use due to  
678 interception losses and year-round transpiration potential (Fig. S9c). Consequently, the implications for both  
679 reduced groundwater recharge and reduced forest productivity has encouraged landowners to explore alternative  
680 land use, such as broadleaves forests and agroforestry. These options have the potential for optimizing biomass  
681 productivity and land use resilience with increased landscape water retention and increased groundwater recharge.

682 These results (e.g., Figs. 8 and S10) have practical applications, such as estimating the direction and magnitude  
683 of the changes in evapotranspiration and water yield as a function of forest management practices, driven by  
684 alterations in canopy structure and rooting depth. The modelling approach thus provides useful insights into the  
685 hydrological implications of alternative canopy structures and rooting patterns for water use. Figure 12 compares  
686 the mean annual partitioning of water fluxes and soil moisture across broadleaf, coniferous, and agroforest types  
687 under dry and wet year conditions. It highlights how different vegetation strategies influence hydrological  
688 resilience, with substantial differences in water partitioning observed between dry and wet years across contrasting  
689 forest management scenarios. By simulating long-term water availability across periods of alternating wet and dry  
690 conditions, EcoPlot-iso simulations suggest that mixed forests and agroforestry can enhance water supply  
691 resilience in drought-sensitive catchments by sustaining both water yield and groundwater recharge.

692



693

694 **Figure 12.** Comparison of mean annual water fluxes and soil moisture in the upper, lower, and deeper layers for  
 695 Broadleaf (a), Coniferous (b), and Agroforest (c) forests under dry (2006, 2018, 2022) and wet (2002, 2007,  
 696 2010, 2023) year conditions.

## 697 **5.2 Soil Moisture Dynamics and Root Water Uptake Processes across Forest Management Scenarios**

698 At most of the monitoring plots in the DMC, groundwater is typically more than 3 meters below the ground surface  
699 (Ying et al., 2025). Therefore, except in older forest plots with deeply rooting trees, vegetation relies on soil  
700 moisture for root water uptake. Even for mature trees, there is evidence that most root water uptake occurs in the  
701 near-surface soil horizons, as demonstrated by Birkel et al. (2025), 20 km from the DMC. A global synthesis by  
702 Evaristo & McDonnell (2017) further supports this, indicating that ~77% of plant water uptake comes from  
703 shallow sources, with deeper groundwater use primarily in more arid regions. While hydraulic redistribution may  
704 provide deeper access for some species (Emerman & Dawson, 1996), rooting strategies are complex and highly  
705 species-specific (Demir et al., 2024). In this context, our results highlight the intermediate soil layer (10–30 cm)  
706 as the most reactive and significant for sustaining transpiration, with anomaly magnitudes nearly twice those of  
707 both the shallow (0–10 cm) and deeper (30–60 cm) layers across all forest types.

708 In addition, seasonal comparisons revealed that summer soil moisture anomalies were more negative than those  
709 in spring for all forest types (Fig. S12). This is likely linked to higher temperatures and evapotranspiration during  
710 summer, which intensify water stress and drive seasonal variation in soil moisture availability. Forest density and  
711 rooting characteristics substantially influenced the relative magnitude of soil moisture anomalies (Figs. S13 and  
712 S14, respectively). Denser forests exhibited stronger negative anomalies during dry periods and enhanced positive  
713 anomalies in wet periods, amplifying seasonal fluctuations. For example, high-density (LAI scaling factor 1.6)  
714 conifer stands showed relative anomalies up to 25% greater than their low-density counterparts (Fig. S14). In  
715 contrast, shallow-rooted systems moderated this response, leading to more stable soil moisture dynamics. Among  
716 the management scenarios, agroforestry consistently exhibited the smallest anomalies, reflecting greater buffering  
717 capacity and higher ecohydrological resilience.

718 The improved rooting scheme in EcoPlot-iso represents depth-dependent transpiration by dynamically linking  
719 root water uptake efficiency to soil moisture availability across three soil compartments (see Section 3.2). Unlike  
720 models such as RHESSys and ECH2O, which partition a prescribed total transpiration—typically derived from  
721 the energy balance—across layers based on static root distributions, our approach allows transpiration to emerge  
722 from potential evapotranspiration, root-zone constraints, and soil moisture availability. The aim was not to  
723 optimize species-specific root dynamics, but to represent the relative influence of rooting depth on water uptake  
724 and partitioning, particularly in shallow-rooted or structurally diverse systems such as young forests. While the  
725 new implementation improves the process representation of root–soil interactions, it did not result in a substantial  
726 improvement in simulated soil moisture. For shallow vegetation types such as grasslands and croplands, model  
727 performance—measured using the mKGE was similar with and without the new transpiration function (results  
728 not shown). Moreover, direct validation of the root uptake scheme remains challenging due to the lack of  
729 supporting observations, such as root distribution data, xylem water isotopes, or sap flux measurements.  
730 Addressing this issue is a clear priority for future research.

731 These findings highlight how structurally diverse systems, such as agroforests, enhance the buffering capacity of  
732 ecosystems by improving groundwater recharge and reducing the amplitude of soil moisture fluctuations, thereby  
733 supporting greater resilience during dry periods (Tetzlaff et al., 2024). Together, these insights underscore the  
734 importance of rooting depth, forest structure, and seasonal climate variability in shaping soil moisture patterns

735 and regulating vegetation resilience. Accounting for these factors is essential for informing adaptive forest  
736 management in drought-prone catchments like the DMC.

### 737 **5.3 Advancing Tracer-Aided Ecohydrological Modelling: Challenges and Future Outlook**

738 This study demonstrates that tracer-aided ecohydrological models, such as the isotope-aided EcoPlot-iso, can be  
739 used to effectively quantify the impact of forest management scenarios on water partitioning and ecohydrological  
740 resilience. By distinguishing between evaporation, transpiration, and subsurface water movements using stable  
741 isotopes (Soulsby et al., 2015), the model captures key hydrological responses—including evapotranspiration  
742 (ET), groundwater recharge, and soil moisture dynamics—under varying management strategies. These insights  
743 support evidence-based decision-making in drought-sensitive landscapes.

744 Despite these advances, several challenges remain. Conducted in a 66 km<sup>2</sup> mid-sized basin, this study did not  
745 include land use change induced atmospheric feedbacks—such as changes in albedo, radiative balance, or rainfall  
746 patterns—which are less critical at this scale but become important in larger-scale modeling (Ellison et al., 2012;  
747 Filoso et al., 2017). Moreover, this study applied a multi-objective calibration approach, combined with Monte  
748 Carlo sampling, that equally weighted isotopic and soil moisture data. However, further investigation is needed  
749 in how these observational constraints are balanced and interpreted. Recent advances—such as the  
750 DREAM(LoAX) framework (Wu et al., 2025)—demonstrate how simultaneous calibration and diagnostic  
751 analysis under the equifinality thesis can improve parameter identifiability, model robustness, and process  
752 understanding in tracer-aided ecohydrological models.

753 While this study used  $\delta^2\text{H}$  to constrain evaporative fractionation given, the combined use of  $\delta^{18}\text{O}$  and  $\delta^2\text{H}$  (or d-  
754 excess) may help improve the separation of evaporation effects and mixing processes (e.g. Penna et al., 2018)  
755 though this was beyond the scope of this paper. Many recent studies have used isotopic data to investigate root  
756 water uptake patterns, revealing how tree species, soil properties, and spatial water availability shape plant water  
757 use strategies (Demir et al., 2024; Rothfuss & Javaux, 2017). Integrating tracer-aided models with soil and xylem  
758 water isotope data offers a promising path to improving the representation of root water uptake, which is often  
759 simplified in current modelling approaches (Birkel et al., 2025). Improving root uptake representation requires  
760 consideration of species-specific traits and local soil-water conditions. However, the practical application of such  
761 improvements is limited by the scarcity of soil and xylem water isotope data, which are essential for constraining  
762 root water uptake dynamics but remain rare due to the labor-intensive and technically demanding nature of field  
763 sampling and laboratory analysis (Landgraf et al., 2022; Sprenger et al., 2017). This scarcity hinders the spatial  
764 and temporal resolution of observational data, limiting our ability to refine root water uptake processes in tracer-  
765 aided models.

766 Upscaling from plot to landscape level remains complex due to spatial heterogeneity in vegetation, soils, and  
767 topography. Addressing this requires spatially distributed modeling frameworks that can explicitly capture  
768 heterogeneity in ecohydrological processes across different landscape units (Kuppel et al., 2018; van Huijgevoort  
769 et al., 2016). Enhanced integration with remote sensing techniques can also help address these scaling limitations  
770 by providing spatially continuous data on vegetation dynamics, soil moisture, and ET (Yang et al., 2023).  
771 Incorporating ET observations, for instance, could strengthen model interpretation of flux dynamics. Currently,  
772 key processes such as lateral subsurface flows and upward capillary fluxes are not explicitly represented in the

773 EcoPlot-iso model. Including these components, along with improved representation of groundwater-surface  
774 water interactions, could improve simulations of water connectivity and storage resilience.

775 It is important to note that the scenario framework presented here is intentionally exploratory and management-  
776 oriented, rather than species-specific. While EcoPlot-iso captures key controls on water partitioning through  
777 canopy structure, soil moisture dynamics, and tracer-based separation of fluxes, additional physiological traits—  
778 such as stomatal regulation, vapor pressure deficit (VPD) sensitivity, and species-specific drought stress  
779 strategies—are not explicitly represented. These processes are known to influence transpiration dynamics and  
780 vegetation responses to drought, and their inclusion represents an important direction for future model  
781 development. Accordingly, the results of this study are interpreted in a relative sense, emphasizing comparative  
782 responses and management-relevant trade-offs rather than absolute or species-level predictions.

## 783 **6 Conclusion and Outlook**

784 The tracer-aided ecohydrological model EcoPlot-iso was applied to quantify how alternative forest management  
785 scenarios influence long-term water partitioning and ecohydrological resilience in the drought-sensitive  
786 Demnitzer Millcreek catchment (DMC), northeastern Germany. Baseline simulations for the period 2000–2024  
787 were established at three forest sites (broadleaf forest, conifer forest, and agroforestry) and successfully  
788 reproduced observed soil moisture and soil water isotope ( $\delta^2\text{H}$ ) dynamics through a multi-criteria calibration  
789 approach. A key development in this study was the integration of a depth-dependent root water uptake function,  
790 which enable the representation of transpiration across soil layers associated with contrasting rooting distributions  
791 and stand ages. Building on these baseline simulations, a generic scenario framework was applied to  
792 systematically assess the effects of forest type, forest density, and rooting characteristics on evapotranspiration,  
793 groundwater recharge, and soil moisture dynamics under contrasting dry and wet climatic conditions.

794 The results revealed clear trade-offs between evapotranspiration (ET) and groundwater recharge across different  
795 forest management scenarios. On average, conifer forest exhibited higher ET, approximately 7–11% greater than  
796 broadleaf forest and agroforestry, accompanied by reduced groundwater recharge, particularly during low-flow  
797 periods. In contrast, agroforestry buffered drought stress, maintained lower soil moisture variability, and enhanced  
798 groundwater recharge. Conifers showed the strongest soil moisture anomalies, indicating greater drought  
799 sensitivity, while agroforests exhibited the most stable soil water storage. The intermediate soil layer (10–30 cm)  
800 was identified as the most responsive zone, consistently exhibiting the largest anomalies due to its role as the  
801 dominant root water uptake region supporting transpiration.

802 Beyond advancing process understanding, this study provided a practical and transferable framework for land  
803 management. By incorporating key controls such as canopy properties and root distribution, EcoPlot-iso facilitates  
804 an accessible means of assessing long-term land management impacts on landscape ecohydrology. The  
805 visualization and decision-support framework developed here offers a transparent, scenario-based platform for  
806 evaluating forest management strategies in climate-sensitive regions. These tools are well-suited for informing  
807 resilient land use planning under increasing climate variability.

808 Looking ahead, future research could usefully aim to incorporate additional isotopic tracers—such as deeper soil  
809 water (> 1 m), groundwater, and xylem water isotopes—to further constrain root water uptake functions and

810 capture their variability across species and hydroclimatic conditions. The integration of high-resolution remote  
811 sensing data—particularly LiDAR for detailed characterization of forest structure—will enhance model  
812 parameterization and improve the spatial representation of heterogeneity in canopy height, leaf area distribution,  
813 and forest density. Advancing the EcoPlot-iso framework to incorporate lateral subsurface flows, groundwater  
814 dynamics, and coupled land–atmosphere feedbacks will support broader applications, including the assessment of  
815 large-scale land use change. Collectively, these developments will enhance model robustness and enable more  
816 informed, resilient land and water management strategies under a warming climate.

#### 817 **Code and data availability**

818 The data and code that support the findings of this study are available from the corresponding author upon  
819 reasonable request.

#### 820 **Author contribution**

821 CJ contributed to the methodology, software development, formal analysis, investigation, visualization, and  
822 writing of the original draft. DT contributed to conceptualization, investigation, data curation, validation,  
823 resources, project administration, and funding acquisition. SW contributed to methodology, investigation and data  
824 curation. CB contributed to software, methodology, and resources. HL contributed to investigation, visualization  
825 and validation. CS contributed to conceptualization, methodology, validation, investigation. All authors  
826 contributed to writing – review and editing.

#### 827 **Competing interests**

828 The authors declare that they have no conflict of interest.

#### 829 **Acknowledgements**

830 Tetzlaff's contributions were partly funded through the WETSCAPES2.0 project (DFG TRR410/1 2025). Tetzlaff  
831 also received funding from the "Wasserressourcenpreis 2024" awarded by the Rüdiger Kurt Bode-Foundation.  
832 Contributions from Soulsby were supported by Leibnitz Association Germany in the project Wetland Restoration  
833 in Peatlands. Laudon was funded by KAW 2018.0259 and 2023.0245, and Soulsby was also funded as an  
834 International KSLA Guest Professor at SLU by the Wallenberg Foundation (WP2023-0001). Birkel would like to  
835 thank the IGB for generously supporting him with a senior fellowship and the UCR for a sabbatical license. We  
836 extend our appreciation to Benedikt Boesel and the team from the Finck Foundation ([www.finck-stiftung.org](http://www.finck-stiftung.org)) for  
837 their collaborative support and for granting access to study sites. The authors are very grateful for the constructive  
838 comments provided by the Editor, Prof. Dr. Anke Hildebrandt, and two anonymous reviewers.

#### 839 **Reference**

840 Ault, T. R. (2020). On the essentials of drought in a changing climate. In *Science* (Vol. 368, Number 6488).  
841 <https://doi.org/10.1126/science.aaz5492>

- 842 Birkel, C., Arciniega-Esparza, S., Maneta, M. P., Boll, J., Stevenson, J. L., Benegas-Negri, L., Tetzlaff, D., &  
843 Soulsby, C. (2024). Importance of measured transpiration fluxes for modelled ecohydrological partitioning  
844 in a tropical agroforestry system. *Agricultural and Forest Meteorology*, 346.  
845 <https://doi.org/10.1016/j.agrformet.2023.109870>
- 846 Birkel, C., Tetzlaff, D., Ring, A. M., & Soulsby, C. (2025). Does high resolution in situ xylem and atmospheric  
847 vapor isotope data help improve modeled estimates of ecohydrological partitioning? *Agricultural and*  
848 *Forest Meteorology*, 365. <https://doi.org/10.1016/j.agrformet.2025.110467>
- 849 Bonan, G. B. (2008). Forests and climate change: Forcings, feedbacks, and the climate benefits of forests. In  
850 *Science* (Vol. 320, Number 5882). <https://doi.org/10.1126/science.1155121>
- 851 Bosch, J. M., & Hewlett, J. D. (1982). A REVIEW OF CATCHMENT EXPERIMENTS TO DETERMINE THE  
852 EFFECT OF VEGETATION CHANGES ON WATER YIELD AND EVAPOTRANSPIRATION. In  
853 *Journal of Hydrology* (Vol. 55).
- 854 Brauman, K. A., Freyberg, D. L., & Daily, G. C. (2010). Forest structure influences on rainfall partitioning and  
855 cloud interception: A comparison of native forest sites in Kona, Hawai'i. *Agricultural and Forest*  
856 *Meteorology*, 150(2). <https://doi.org/10.1016/j.agrformet.2009.11.011>
- 857 Brown, A. E., Western, A. W., McMahon, T. A., & Zhang, L. (2013). Impact of forest cover changes on annual  
858 streamflow and flow duration curves. *Journal of Hydrology*, 483.  
859 <https://doi.org/10.1016/j.jhydrol.2012.12.031>
- 860 Brown, A. E., Zhang, L., McMahon, T. A., Western, A. W., & Vertessy, R. A. (2005). A review of paired  
861 catchment studies for determining changes in water yield resulting from alterations in vegetation. *Journal*  
862 *of Hydrology*, 310(1–4), 28–61. <https://doi.org/10.1016/j.jhydrol.2004.12.010>
- 863 Calder, I. R. (1998). Water use by forests, limits and controls. *Tree Physiology*, 18(8–9).  
864 <https://doi.org/10.1093/treephys/18.8-9.625>
- 865 Demir, G., Guswa, A. J., Filipzik, J., Metzger, J. C., Römermann, C., & Hildebrandt, A. (2024). Root water uptake  
866 patterns are controlled by tree species interactions and soil water variability. *Hydrology and Earth System*  
867 *Sciences*, 28(6), 1441–1461. <https://doi.org/10.5194/hess-28-1441-2024>
- 868 Douinot, A., Tetzlaff, D., Maneta, M., Kuppel, S., Schulte-Bisping, H., & Soulsby, C. (2019). Ecohydrological  
869 modelling with ECH2O-iso to quantify forest and grassland effects on water partitioning and flux ages.  
870 *Hydrological Processes*, 33(16), 2174–2191. <https://doi.org/10.1002/hyp.13480>
- 871 Dubbert, M., Couvreur, V., Kübert, A., & Werner, C. (2023). Plant water uptake modelling: added value of cross-  
872 disciplinary approaches. In *Plant Biology* (Vol. 25, Number 1). <https://doi.org/10.1111/plb.13478>
- 873 Ellison, D., Futter, M. N., & Bishop, K. (2012). On the forest cover-water yield debate: From demand- to supply-  
874 side thinking. In *Global Change Biology* (Vol. 18, Number 3). [https://doi.org/10.1111/j.1365-](https://doi.org/10.1111/j.1365-2486.2011.02589.x)  
875 [2486.2011.02589.x](https://doi.org/10.1111/j.1365-2486.2011.02589.x)
- 876 Emerman, S. H., & Dawson, T. E. (1996). Hydraulic lift and its influence on the water content of the rhizosphere:  
877 An example from sugar maple, *Acer saccharum*. *Oecologia*, 108(2). <https://doi.org/10.1007/BF00334651>
- 878 Estrela, T., & Vargas, E. (2012). Drought Management Plans in the European Union. The Case of Spain. In *Water*  
879 *Resources Management* (Vol. 26, Number 6). <https://doi.org/10.1007/s11269-011-9971-2>
- 880 Evaristo, J., & McDonnell, J. J. (2017). Prevalence and magnitude of groundwater use by vegetation: A global  
881 stable isotope meta-analysis. *Scientific Reports*, 7. <https://doi.org/10.1038/srep44110>
- 882 Falkenmark, M., & Rockström, J. (2006). The New Blue and Green Water Paradigm: Breaking New Ground for  
883 Water Resources Planning and Management. *Journal of Water Resources Planning and Management*,  
884 132(3). [https://doi.org/10.1061/\(asce\)0733-9496\(2006\)132:3\(129\)](https://doi.org/10.1061/(asce)0733-9496(2006)132:3(129))

- 885 Fatichi, S., Ivanov, V. Y., & Caporali, E. (2012). A mechanistic ecohydrological model to investigate complex  
886 interactions in cold and warm water-controlled environments: 1. Theoretical framework and plot-scale  
887 analysis. *Journal of Advances in Modeling Earth Systems*, 4(5). <https://doi.org/10.1029/2011MS000086>
- 888 Filoso, S., Bezerra, M. O., Weiss, K. C. B., & Palmer, M. A. (2017). Impacts of forest restoration on water yield:  
889 A systematic review. In *PLoS ONE* (Vol. 12, Number 8). <https://doi.org/10.1371/journal.pone.0183210>
- 890 Gelbrecht, J., Driescher, E., Lademann, H., Schönfelder, J., & Exner, H.-J. (1996). Diffuse nutrient impact on  
891 surface water bodies and its abatement by restoration measures in a small catchment area in North-East  
892 Germany. *Water Science and Technology*, 33(4–5). <https://doi.org/10.2166/wst.1996.0501>
- 893 Gelbrecht, J., Lengsfeld, H., Pöthig, R., & Opitz, D. (2005). Temporal and spatial variation of phosphorus input,  
894 retention and loss in a small catchment of NE Germany. *Journal of Hydrology*, 304(1–4), 151–165.  
895 <https://doi.org/10.1016/j.jhydrol.2004.07.028>
- 896 Geris, J., Tetzlaff, D., McDonnell, J., & Soulsby, C. (2015). The relative role of soil type and tree cover on water  
897 storage and transmission in northern headwater catchments. *Hydrological Processes*, 29(7).  
898 <https://doi.org/10.1002/hyp.10289>
- 899 Guswa, A. J., Tetzlaff, D., Selker, J. S., Carlyle-Moses, D. E., Boyer, E. W., Bruen, M., Cayuela, C., Creed, I. F.,  
900 van de Giesen, N., Grasso, D., Hannah, D. M., Hudson, J. E., Hudson, S. A., Iida, S., Jackson, R. B., Katul,  
901 G. G., Kumagai, T., Llorens, P., Lopes Ribeiro, F., ... Levina, D. F. (2020). Advancing ecohydrology in the  
902 21st century: A convergence of opportunities. In *Ecohydrology* (Vol. 13, Number 4). John Wiley and Sons  
903 Ltd. <https://doi.org/10.1002/eco.2208>
- 904 Hersbach, H., Bell, B., Berrisford, P., Hirahara, S., Horányi, A., Muñoz-Sabater, J., Nicolas, J., Peubey, C., Radu,  
905 R., Schepers, D., Simmons, A., Soci, C., Abdalla, S., Abellan, X., Balsamo, G., Bechtold, P., Biavati, G.,  
906 Bidlot, J., Bonavita, M., ... Thépaut, J.-N. (2020). The ERA5 global reanalysis. *Quarterly Journal of the*  
907 *Royal Meteorological Society*, 146(730), 1999–2049. <https://doi.org/https://doi.org/10.1002/qj.3803>
- 908 Hibbert, A. R. (1967). Forest Treatment Effects on Water Yield. *International Symposium For Hydrology*.
- 909 Huntington, T. G. (2006). Evidence for intensification of the global water cycle: Review and synthesis. *Journal*  
910 *of Hydrology*, 319(1–4), 83–95. <https://doi.org/10.1016/j.jhydrol.2005.07.003>
- 911 Kleine, L., Tetzlaff, D., Smith, A., Dubbert, M., & Soulsby, C. (2021). Modelling ecohydrological feedbacks in  
912 forest and grassland plots under a prolonged drought anomaly in Central Europe 2018–2020. *Hydrological*  
913 *Processes*, 35(8). <https://doi.org/10.1002/hyp.14325>
- 914 Kling, H., Fuchs, M., & Paulin, M. (2012). Runoff conditions in the upper Danube basin under an ensemble of  
915 climate change scenarios. *Journal of Hydrology*, 424–425. <https://doi.org/10.1016/j.jhydrol.2012.01.011>
- 916 Knighton, J., Kuppel, S., Smith, A., Soulsby, C., Sprenger, M., & Tetzlaff, D. (2020). Using isotopes to  
917 incorporate tree water storage and mixing dynamics into a distributed ecohydrologic modelling framework.  
918 *Ecohydrology*, 13(3). <https://doi.org/10.1002/eco.2201>
- 919 Knighton, J., Sanchez-Martinez, P., & Anderegg, L. (2024). A global dataset of tree hydraulic and structural traits  
920 imputed from phylogenetic relationships. *Scientific Data*, 11(1). <https://doi.org/10.1038/s41597-024-04254-4>
- 922 Kool, D., Agam, N., Lazarovitch, N., Heitman, J. L., Sauer, T. J., & Ben-Gal, A. (2014). A review of approaches  
923 for evapotranspiration partitioning. In *Agricultural and Forest Meteorology* (Vol. 184).  
924 <https://doi.org/10.1016/j.agrformet.2013.09.003>
- 925 Kumar, R., Shankar, V., & Jat, M. K. (2015). Evaluation of root water uptake models - A review. In *ISH Journal*  
926 *of Hydraulic Engineering* (Vol. 21, Number 2). <https://doi.org/10.1080/09715010.2014.981955>
- 927 Kuppel, S., Tetzlaff, D., Maneta, M. P., & Soulsby, C. (2018). Ech2O-iso 1.0: Water isotopes and age tracking  
928 in a process-based, distributed ecohydrological model. *Geoscientific Model Development*, 11(7), 3045–3069.  
929 <https://doi.org/10.5194/gmd-11-3045-2018>

- 930 Landgraf, J., Tetzlaff, D., Birkel, C., Stevenson, J. L., & Soulsby, C. (2023). Assessing land use effects on  
 931 ecohydrological partitioning in the critical zone through isotope-aided modelling. *Earth Surface Processes  
 932 and Landforms*, 48(15), 3199–3219. <https://doi.org/10.1002/esp.5691>
- 933 Landgraf, J., Tetzlaff, D., Wu, S., Freymüller, J., & Soulsby, C. (2022). Using stable water isotopes to understand  
 934 ecohydrological partitioning under contrasting land uses in a drought-sensitive rural, lowland catchment.  
 935 *Hydrological Processes*, 36(12). <https://doi.org/10.1002/hyp.14779>
- 936 Luo, S., Tetzlaff, D., Smith, A., & Soulsby, C. (2024). Assessing impacts of alternative land use strategies on  
 937 water partitioning, storage and ages in drought-sensitive lowland catchments using tracer-aided  
 938 ecohydrological modelling. *Hydrological Processes*, 38(4). <https://doi.org/10.1002/hyp.15126>
- 939 Mahmood, R., Pielke, R. A., Hubbard, K. G., Niyogi, D., Dirmeyer, P. A., McAlpine, C., Carleton, A. M., Hale,  
 940 R., Gameda, S., Beltrán-Przekurat, A., Baker, B., Mcnider, R., Legates, D. R., Shepherd, M., Du, J., Blanken,  
 941 P. D., Frauenfeld, O. W., Nair, U. S., & Fall, S. (2014). Land cover changes and their biogeophysical effects  
 942 on climate. *International Journal of Climatology*, 34(4). <https://doi.org/10.1002/joc.3736>
- 943 McKay, M. D., Beckman, R. J., & Conover, W. J. (1979). Comparison of three methods for selecting values of  
 944 input variables in the analysis of output from a computer code. *Technometrics*, 21(2).  
 945 <https://doi.org/10.1080/00401706.1979.10489755>
- 946 Neill, A. J., Birkel, C., Maneta, M. P., Tetzlaff, D., & Soulsby, C. (2021). Structural changes to forests during  
 947 regeneration affect water flux partitioning, water ages and hydrological connectivity: Insights from tracer-  
 948 aided ecohydrological modelling. *Hydrology and Earth System Sciences*, 25(9), 4861–4886.  
 949 <https://doi.org/10.5194/hess-25-4861-2021>
- 950 Orth, R., & Destouni, G. (2018). Drought reduces blue-water fluxes more strongly than green-water fluxes in  
 951 Europe. *Nature Communications*, 9(1). <https://doi.org/10.1038/s41467-018-06013-7>
- 952 Penna, D., Hopp, L., Scandellari, F., Allen, S. T., Benettin, P., Beyer, M., Geris, J., Klaus, J., Marshall, J. D.,  
 953 Schwendenmann, L., Volkmann, T. H. M., Von Freyberg, J., Amin, A., Ceperley, N., Engel, M., Frentress,  
 954 J., Giambastiani, Y., McDonnell, J. J., Zuecco, G., ... Kirchner, J. W. (2018). Ideas and perspectives:  
 955 Tracing terrestrial ecosystem water fluxes using hydrogen and oxygen stable isotopes - Challenges and  
 956 opportunities from an interdisciplinary perspective. *Biogeosciences*, 15(21). <https://doi.org/10.5194/bg-15-6399-2018>
- 958 Pielke, R. A., Pitman, A., Niyogi, D., Mahmood, R., McAlpine, C., Hossain, F., Goldewijk, K. K., Nair, U., Betts,  
 959 R., Fall, S., Reichstein, M., Kabat, P., & de Noblet, N. (2011). Land use/land cover changes and climate:  
 960 Modeling analysis and observational evidence. In *Wiley Interdisciplinary Reviews: Climate Change* (Vol.  
 961 2, Number 6). <https://doi.org/10.1002/wcc.144>
- 962 Quandt, A., Neufeldt, H., & Gorman, K. (2023). Climate change adaptation through agroforestry: opportunities  
 963 and gaps. In *Current Opinion in Environmental Sustainability* (Vol. 60).  
 964 <https://doi.org/10.1016/j.cosust.2022.101244>
- 965 Ricci, G. F., De Girolamo, A. M., & Gentile, F. (2020). Modeling the Effect of Different Management Practices  
 966 for Soil Erosion Control in a Mediterranean Watershed. *Lecture Notes in Civil Engineering*, 67(June), 125–  
 967 132. [https://doi.org/10.1007/978-3-030-39299-4\\_14](https://doi.org/10.1007/978-3-030-39299-4_14)
- 968 Rothfuss, Y., & Javaux, M. (2017). Reviews and syntheses: Isotopic approaches to quantify root water uptake: A  
 969 review and comparison of methods. *Biogeosciences*, 14(8). <https://doi.org/10.5194/bg-14-2199-2017>
- 970 Shen, H., Tolson, B. A., & Mai, J. (2022). Time to Update the Split-Sample Approach in Hydrological Model  
 971 Calibration. *Water Resources Research*, 58(3). <https://doi.org/10.1029/2021WR031523>
- 972 Smith, A., Tetzlaff, D., Gelbrecht, J., Kleine, L., & Soulsby, C. (2020). Riparian wetland rehabilitation and beaver  
 973 re-colonization impacts on hydrological processes and water quality in a lowland agricultural catchment.  
 974 *Science of the Total Environment*, 699. <https://doi.org/10.1016/j.scitotenv.2019.134302>

- 975 Smith, A., Tetzlaff, D., Kleine, L., Maneta, M., & Soulsby, C. (2021). Quantifying the effects of land use and  
976 model scale on water partitioning and water ages using tracer-aided ecohydrological models. *Hydrology  
977 and Earth System Sciences*, 25(4), 2239–2259. <https://doi.org/10.5194/hess-25-2239-2021>
- 978 Soulsby, C., Birkel, C., Geris, J., Dick, J., Tunaley, C., & Tetzlaff, D. (2015). Stream water age distributions  
979 controlled by storage dynamics and nonlinear hydrologic connectivity: Modeling with high-resolution  
980 isotope data. *Water Resources Research*, 51(9). <https://doi.org/10.1002/2015WR017888>
- 981 Sprenger, M., Tetzlaff, D., & Soulsby, C. (2017). Soil water stable isotopes reveal evaporation dynamics at the  
982 soil-plant-atmosphere interface of the critical zone. *Hydrology and Earth System Sciences*, 21(7).  
983 <https://doi.org/10.5194/hess-21-3839-2017>
- 984 Sterling, S. M., Ducharne, A., & Polcher, J. (2013). The impact of global land-cover change on the terrestrial  
985 water cycle. *Nature Climate Change*, 3(4). <https://doi.org/10.1038/nclimate1690>
- 986 Stevenson, J. L., Birkel, C., Comte, J. C., Tetzlaff, D., Marx, C., Neill, A., Maneta, M., Boll, J., & Soulsby, C.  
987 (2023). Quantifying heterogeneity in ecohydrological partitioning in urban green spaces through the  
988 integration of empirical and modelling approaches. *Environmental Monitoring and Assessment*, 195(4).  
989 <https://doi.org/10.1007/s10661-023-11055-6>
- 990 Tague, C. L., & Band, L. E. (2004). RHESSys: Regional Hydro-Ecologic Simulation System—An Object-  
991 Oriented Approach to Spatially Distributed Modeling of Carbon, Water, and Nutrient Cycling. *Earth  
992 Interactions*, 8(19). [https://doi.org/10.1175/1087-3562\(2004\)8<1:rhss>2.0.co;2](https://doi.org/10.1175/1087-3562(2004)8<1:rhss>2.0.co;2)
- 993 Tetzlaff, D., Carey, S. K., McNamara, J. P., Laudon, H., & Soulsby, C. (2017). The essential value of long-term  
994 experimental data for hydrology and water management. In *Water Resources Research* (Vol. 53, Number  
995 4, pp. 2598–2604). Blackwell Publishing Ltd. <https://doi.org/10.1002/2017WR020838>
- 996 Tetzlaff, D., Laudon, H., Luo, S., & Soulsby, C. (2024). Ecohydrological resilience and the landscape water  
997 storage continuum in droughts. *Nature Water*, 2(10), 915–918. [https://doi.org/10.1038/s44221-024-00300-  
998 y](https://doi.org/10.1038/s44221-024-00300-<br/>
998 y)
- 999 te Wierik, S. A., Cammeraat, E. L. H., Gupta, J., & Artzy-Randrup, Y. A. (2021). Reviewing the Impact of Land  
1000 Use and Land-Use Change on Moisture Recycling and Precipitation Patterns. In *Water Resources Research*  
1001 (Vol. 57, Number 7). <https://doi.org/10.1029/2020WR029234>
- 1002 Trenberth, K. E. (2011). Changes in precipitation with climate change. *Climate Research*, 47(1–2), 123–138.  
1003 <https://doi.org/10.3354/cr00953>
- 1004 van Huijgevoort, M. H. J., Tetzlaff, D., Sutanudjaja, E. H., & Soulsby, C. (2016). Using high resolution tracer  
1005 data to constrain water storage, flux and age estimates in a spatially distributed rainfall-runoff model.  
1006 *Hydrological Processes*, 30(25), 4761–4778. <https://doi.org/10.1002/hyp.10902>
- 1007 Wang-Erlandsson, L., Van Der Ent, R. J., Gordon, L. J., & Savenije, H. H. G. (2014). Contrasting roles of  
1008 interception and transpiration in the hydrological cycle - Part 1: Temporal characteristics over land. *Earth  
1009 System Dynamics*, 5(2). <https://doi.org/10.5194/esd-5-441-2014>
- 1010 Wu, S., Tetzlaff, D., Beven, K., & Soulsby, C. (2025). DREAM(LoAX): Simultaneous Calibration and Diagnosis  
1011 for Tracer-Aided Ecohydrological Models Under the Equifinality Thesis. *Water Resources Research*, 61(3),  
1012 e2024WR038779. <https://doi.org/https://doi.org/10.1029/2024WR038779>
- 1013 Wu, S., Tetzlaff, D., Goldhammer, T., & Soulsby, C. (2021). Hydroclimatic variability and riparian wetland  
1014 restoration control the hydrology and nutrient fluxes in a lowland agricultural catchment. *Journal of  
1015 Hydrology*, 603. <https://doi.org/10.1016/j.jhydrol.2021.126904>
- 1016 Wu, S., Tetzlaff, D., Yang, X., Smith, A., & Soulsby, C. (2023). Integrating Tracers and Soft Data Into Multi-  
1017 Criteria Calibration: Implications From Distributed Modeling in a Riparian Wetland. *Water Resources  
1018 Research*, 59(11). <https://doi.org/10.1029/2023WR035509>
- 1019 Yang, X., Tetzlaff, D., Müller, C., Knöller, K., Borchardt, D., & Soulsby, C. (2023). Upscaling Tracer-Aided  
1020 Ecohydrological Modeling to Larger Catchments: Implications for Process Representation and

1021 Heterogeneity in Landscape Organization. *Water Resources Research*, 59(3).  
1022 <https://doi.org/10.1029/2022WR033033>

1023 Ying, Z., Tetzlaff, D., Comte, J.-C., Wu, S., & Soulsby, C. (2025). Storage Dynamics and Groundwater–Surface  
1024 Water Interactions in a Drought Sensitive Lowland Catchment: Process-Based Modelling as a Learning  
1025 Tool. *Hydrological Processes*, 39(5), e70141. <https://doi.org/https://doi.org/10.1002/hyp.70141>

1026 Yuan, X., Wang, Y., Ji, P., Wu, P., Sheffield, J., & Otkin, J. A. (2023). A global transition to flash droughts under  
1027 climate change. *Science*, 380(6641). <https://doi.org/10.1126/science.abn6301>

1028 Zhang, L., Dawes, W. R., & Walker, G. R. (2001). Response of mean annual evapotranspiration to vegetation  
1029 changes at catchment scale. *Water Resources Research*, 37(3). <https://doi.org/10.1029/2000WR900325>

1030